The influence of heat and freshwater fluxes on convective activity in the Central Irminger Sea

Diploma Thesis
by
Uta Neumann

Mathematisch-Naturwissenschaftliche Fakultät der
Christian-Albrechts-Universität zu Kiel
Kiel, May 2007

Leibniz-Institut für Meereswissenschaften
Düsternbrooker Weg 20, D-24105 Kiel
e-Mail: uneumann@ifm.uni-kiel.de

Summary

Mooring data that have been collected in the Central Irminger Sea between summer 2002 and summer 2006 are evaluated regarding their hydrographic evolution. Different methods are used to estimate the mixed layer depth. During the observation the maximum mixed layer depth with approximately 500 m was measured in winter 2005 which is still above the upper margin of the Labrador Sea Water (LSW) that is found at intermediate depth. Thus no renewal of this water mass took place at the mooring site. A comparison of heat fluxes derived from mooring and NCEP/NCAR reanalyses data reveals an increase in temperature over the upper 1000 m during the observed 4 years. This equals a net heat flux of $4\,\mathrm{W/m^2}$, whereas the oceanic heat transport amounts to $28\,\mathrm{W/m^2}$.
Recent studies using a 1D-model to estimate the development of mixed layer depths showed that deep reaching convection may also occur in this region. They justify the use of the simplified model with the existing conditions. This includes relatively weak mean currents and the cyclonic circulation that traps the water within the Irminger Gyre. The long-term mean of currents measured at the mooring site emphasize the existence of weak mean currents. But due to the variations that are associated with eddies the use of a 1-dimensional model seems not to be appropriate.

Zusammenfassung

Anhand von Verankerungsdaten, die in der Zentralen Irminger See gesammelt wurde, erfolgte eine Auswertung der hydrographischen Eigenschaften der oberen 1500m für den Zeitraum von Sommer 2002 bis Sommer 2006. Die Tiefe der durchmischten Deckschicht wurde unter Verwendung verschiedener Methoden abgeschätzt. Die maximale Tiefe wurde im Winter 2005 mit ca. 500 m erreicht. Dies liegt noch immer oberhalb der Grenze zum LSW, welches in mittleren Tiefen im Irminger Becken anzufinden ist. Es kam somit zu keiner Erneuerung dieser Wassermasse in der Irminger See zum besagten Zeitraum. Ein Vergleich von Wärmeflüssen, die unter Verwendung der Verankerungsdaten und Daten der NCEP/NCAR-Reanalyse bestimmt wurden, ergeben einen Temperaturanstieg der Wassersäule bis 1000 m über den Zeitraum der Beobachtung. Dieser Anstieg ist äquivalent zu einem Nettowärmefluss von $4\,\mathrm{W/m^2}$. Zur gleichen Zeit liefert der ozeanische Transport einen Wärmefluss von $28\,\mathrm{W/m^2}$.
Gegenwärtige Studien, die eindimensionale Modelle zur Berechnung von Deckschichttiefen verwenden, zeigen das tiefreichende Konvektion in dieser Region stattfinden kann. Die Beschränkung auf ein eindimensionales Modell wird damit begründet, dass hier nur geringe Strömungsgeschwindigkeiten zu finden sind und das Wasser durch die zyklonische Zirkulation im Irminger Gyre gefangen bleibt. Das langjährige Mittel der gemessenen Strömungen an der Verankerungsposition bestätigt das Vorhandensein einer geringen mittleren Strömung. Aufgrund der Variationen jedoch, die mit Eddies verbunden sind, scheint die Verwendung eines 1D-Modells nicht angebracht.

Contents

List of Figures

List of Tables

1 Introduction

The steadiness of heat transport from low to high latitudes carried by atmosphere and ocean is very important for the stability of the Earth's climate. Westerlies and trades are the prevailing winds in the mid-latitudes and (sub-)tropics, respectively. Together they build up an Ekman convergence in the mid-latitudes, driving the subtropical gyre. At high latitudes, e.g. in the North Atlantic, the northern side of the westerlies creates an Ekman divergence, driving the subpolar circulation (TOMCZAK AND GODFREY, 2005). At the surface warm waters flow from southern regions to the North Atlantic. Here and in the adjacent seas intense exchange with the atmosphere takes place. The surface water experiences strong cooling and looses heat to the atmosphere which leads to buoyancy loss. The cold water sinks and leaves the area by flowing equatorwards in intermediate and great depths as illustrated in figure 1.2.

There is just a limited number of regions where formation of deep water can take place and the deep ocean is ventilated. Already at the beginning twenties century NANSEN (1912) suggested the Irminger Sea as a potential site where deep convection may occur. Although sporadically mentioned this idea has been neglected for almost 90 years and scientific work focused on investigating convection in the Labrador, Greenland and Mediterranean Seas (amongst others CLARKE AND GASCARD, 1983; MERTENS, 2000; MEDOC GROUP, 1970; VISBECK, 1993; MARSHALL AND SCHOTT, 1999). Meanwhile, the hypothesis that Labrador Sea Water (LSW) may also be formed in the Southern Irminger Sea has been revived and the Irminger Sea basin is now an area of increased interest (e.g. BACON ET AL., 2003; PICKART ET AL., 2003b; VÅGE ET AL., 2006; FALINA, 2007). This is also visible in an increased mooring work activity in this area. Figure 1.1 shows the Irminger Sea and its adjacent regions. The position of the Central Iriminger Sea (CIS) mooring whose data are evaluated in this study is marked. Close to this mooring is an array from the LOCO (*L*ong-Term *O*cean *C*limate *O*bservations)-Programme maintained by the Royal Netherlands Institute for Sea Research and two profiling moorings from the Woods Hole Oceanographic Institution (WHOI). All these mooring sites have been implemented within the last 5 years.

This study will use data provided by the CIS mooring site to estimate the heat and freshwater fluxes that influence the convective activity in the Irminger Sea. In the

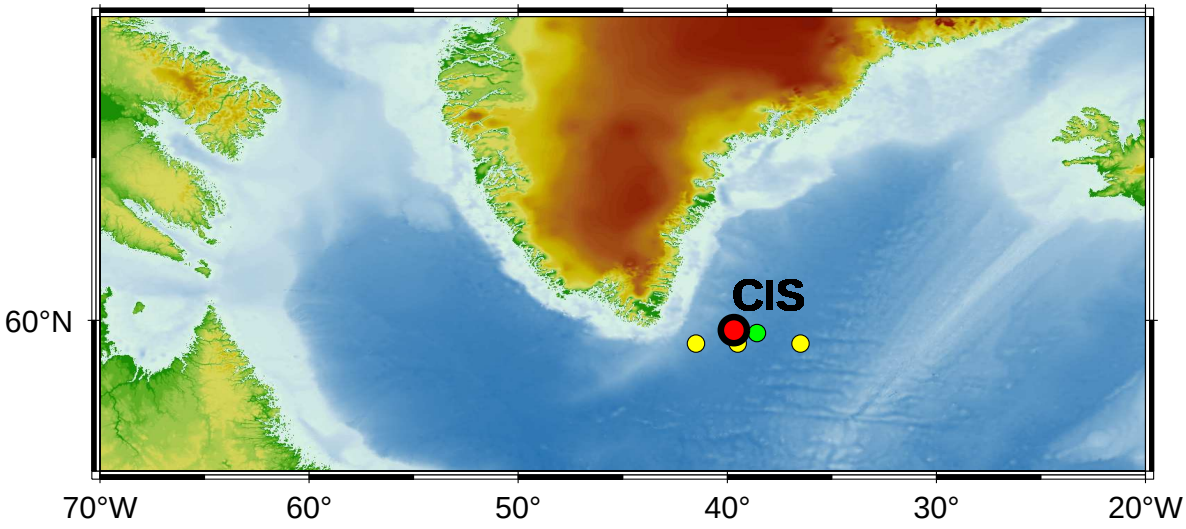

FIGURE 1.1: *Overview of area of interest: the red dot marks the mooring position in the Central Irminger Basin (CIS) that provided data used in this study; yellow and green dots denote mooring positions of the LOCO-programme and from WHOI, respectively.*

following an outline about deep convection in the open ocean and a description of the conditions in the Irminger Sea are presented. In chapter 2 the data used for this study are described. The following chapter contains a description of the mixed-layer properties and development. This includes different estimations of the winterly mixed layer depth. Afterwards, the heat and freshwater budgets and fluxes will be presented and evaluated.

1.1 Deep convection

Deep convection in the open ocean depends on a unique set of atmospheric and oceanic conditions that has to be fulfilled. The process is intermittent in time and involves different scales. Three phases which can be distinguished will briefly be explained here; a detailed discussion is provided by MARSHALL AND SCHOTT (1999).

PHASES OF OCEAN CONVECTION

Preconditioning During preconditioning weakly stratified waters of the interior get close to the surface in consequence of the cyclonic circulation and its associated doming isopycnals. Intense buoyancy loss due to high heat flux and evaporation that increases the salinity erodes the near-surface stratification on large horizontal scale. Thus, the very weakly stratified water underneath is exposed directly to the surface forcing.

Deep Convection Deep convection may be initiated by subsequent cooling events and a considerable part of the water column may overturn in numerous plumes distributing the dense surface water into great depths. Numerical experiment and observations reveals a diameter of less than $1\,\mathrm{km}$ for these plumes that have vertical velocities of up to $10\,\mathrm{m/s}$. Altogether they rapidly mix properties of the convection site and form a homogenous, deeply mixed patch. The scales range from several tens to over hundred kilometres in diameter.

Lateral exchange If the strong forcing stops or the cooling persists over many days, horizontal heat transfers instead of the predominantly vertical transfer happens. The patch laterally exchanges fluid with its surroundings via eddies on geostrophic scales. The mixed fluid spreads out at its neutrally buoyant level under the influence of gravity and rotation. On a timescale of weeks and months it disintegrates and the convection site is reoccupied by adjacent water.

CONDITIONS FOR DEEP CONVECTION

A **weak stratification**, e.g. due to previous convection or advection of weakly stratified water parcels, eases penetration of water motion to great depths.

A **cyclonic circulation** that isolates the water, domes up density surfaces and brings denser, weakly stratified underlying waters closer to the sea surface so that they can directly be exposed to intense surface forcing.

Strong atmospheric forcing due to thermal and / or haline surface fluxes. Therefore open ocean regions that are close to boundaries where cold and dry air is blown from land or ice surfaces over water leading to large sensible and latent heat fluxes are privileged. A high heat flux is necessary to drive the enormous motions that enable water parcels to get through remaining stratification and reach large depths. Strong, cold and dry winds support these conditions. They occur in autumn and winter months during a positive North Atlantic Oscillation (NAO) phase. The NAO is a climatic phenomenon in the North Atlantic Ocean. It represents the fluctuations in the difference of sea-level pressure between the Icelandic Low and the Azores high which controls the strength and direction of westerly winds and storm tracks across the North Atlantic.

Consequently, whether and when deep convection takes place depends on the initial stratification, especially on the established mixed layer at the end of the summer, the meteorological conditions and the role of lateral fluxes that may stratify and stabilize the water column. Due to the variability of mentioned conditions the

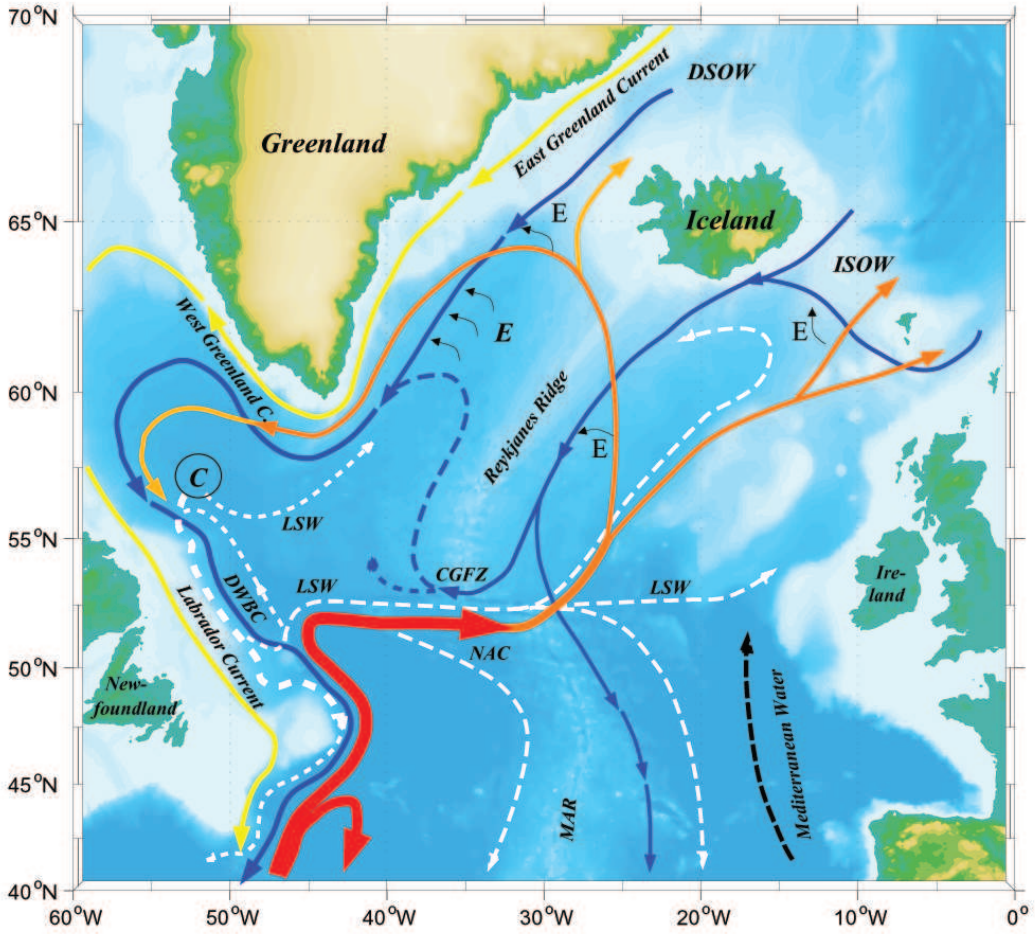

FIGURE 1.2: *Revised schematic illustration of surface (red, orange & yellow), intermediate (white & black) and deep (blue) circulation in the subpolar North Atlantic. Locations of convection (C), entrainment (E), the Mid Atlantic Ridge (MAR) and Charlie Gibbs Fracture Zone (CGFZ) that connects the basin east and west of the MAR are indicated. (from* SFB 460 *(2007))*

deep convection, and hence the deep water formation itself, is not a steady state process that occurs every year and shows great variability in intensity on interannual and decadal timescales.

1.2 The Irminger Sea

The following section contains a brief overview of the study area. The Irminger Sea basin south-eastern of Greenland is isolated by the continent itself, the Reykjanes Ridge in the southeast and the Denmark Strait in the northeast; at the southwest the basin is open. The Irminger Sea is dominated by a cyclonic circulation that is part of the Subpolar Gyre (see figure 1.2). It is enclosed by the near-surface

flowing Irminger Current (IC). Closer to the land, along the shelf break flows the East Greenland Current (EGC) that transports cold, fresh water coming from the Nordic Seas. The Irminger Current is more saline because it is one branch of the northward flowing branch of the North Atlantic Current (NAC) that became slightly diluted. Furthermore, the Deep Western Boundary Current (DWBC) flows along the bottom topography.

The cyclonic circulation leads to doming isopycnals and is one of the conditions that has to be fulfilled to make deep convection possible. As shown by numerous recent studies (amongst others PICKART ET AL., 2003a; BACON ET AL., 2003; VÅGE ET AL., 2006; FALINA, 2007), deep convection indeed occur sporadically in the Irminger Sea although the mean stratification is weaker than in the Labrador Sea and makes it less predestinated. Nevertheless the most important difference to the Labrador Sea is the lack of dry, cold continental air that blows constantly from the Canadian Archipelago in winter time that enhance the turbulent heat fluxes. On the way to the Irminger Sea these air parcels cross the Labrador Sea and get modified. The warms up and moistens, and hence can not cause high surface heat fluxes in the Irminger Sea. Moreover, the reservoir over the Greenland plateau is much smaller as it could provide a sufficient volume of cold air to this area. A capable mechanism to enhance the necessary heat fluxes is a winterly wind pattern called Greenland tip jet, a sporadic but strong and narrow westerly wind blowing off Greenland over the ocean (DOYLE AND SHAPIRO, 1999; PICKART ET AL., 2003a). This phenomenon occurs more often during periods of high NAO index when the storm track is shifted northeastward (MOORE, 2003). The generation of the tip jet is still not fully understood. While MOORE AND RENFREW (2005) suggest formation through an acceleration of air parcels after being deflected around the southern tip of Greenland, DOYLE AND SHAPIRO (1999) explain the formation by air parcels descending directly from the altitude of the Greenland plateau, regulated by conservation of Bernoulli function.

The main profile of the Irminger Sea can be parted into five domains (see figure 1.3). Beneath the seasonally variable mixed layer at about 200 to $500\,\mathrm{m}$ we see a relatively salty and warm ($4\,^{\circ}$-$6\,^{\circ}\mathrm{C}$) water mass. This water is referred to as Irminger Sea Water (ISW), a near-surface water that leaves the basin southward and influences the water in the Labrador Sea at depth between 200-$700\,\mathrm{m}$ (SCHMIDT, 2003). At intermediate depth between approximately 500 and $2000\,\mathrm{m}$ Labrador Sea Water (LSW) is spreading. It is formed by deep convection in the Labrador Sea. The appearance of two salinity minima at about 800 and $1700\,\mathrm{m}$ indicates the presence of both LSW modes - upper and lower LSW (uLSW, lLSW). A comparison of LSW properties (FALINA, 2007) revealed a transit time for LSW from the Labrador Sea to reach the Irminger Sea of about 2 years while according to former estimates (SY

ET AL., 1997; KOLTERMANN ET AL., 1999) that supposed the Labrador Sea is the only source of LSW, the transition takes only 6 months. Therefore, the most recent study emphasizes the concept that the Irminger Sea is an additional source of LSW. This influences the hitherto existing understanding of the ventilation of the North Atlantic and its branch of the meridional overturning circulation (VÅGE ET AL., 2007). Beneath $2000\,\mathrm{m}$ the basin is filled with North East Atlantic Deep Water (NEADW) that is colder and more saline. It has its origin in the eastern basin of the North Atlantic. A mixture of Iceland Scotland Overflow and Mediterranean Waters find its way into the western basin through the Charlie Gibbs Fracture Zone (GFZ) where it likely flows northward following the bottom topography before it becomes a part of the cyclonic circulation in the Irminger Sea basin and contributes to the DWBC. The precise pathway is still unproven. The deepest water mass in the basin is the relatively cold Denmark Strait Overflow Water (DSOW) that overflows the Denmark Strait sill and flows afterwards southward with the DWBC along the bottom topography.

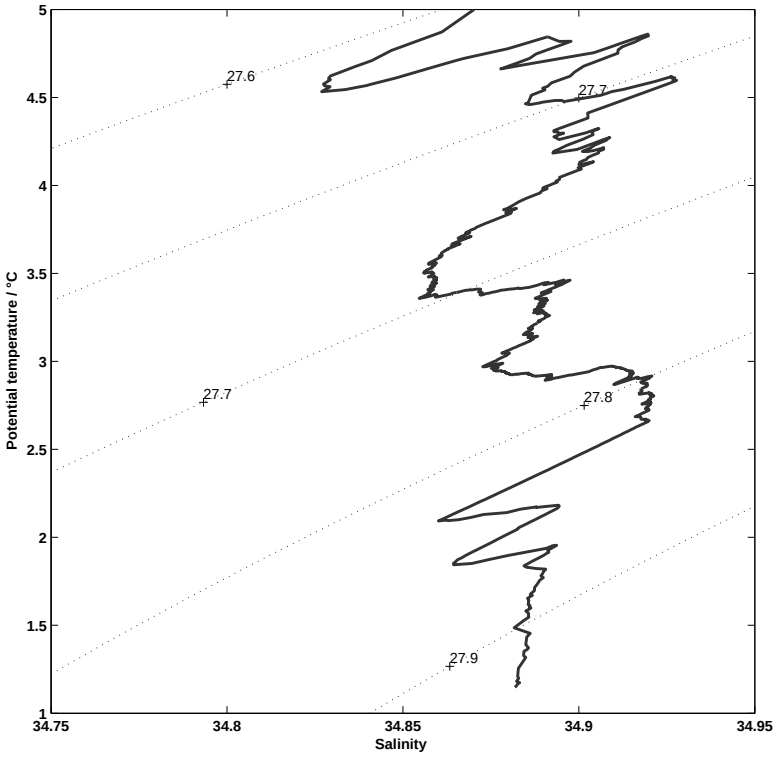

FIGURE 1.3: *Diagram of potential temperature and salinity data measured by a CTD cast that was taken close to the mooring site in summer 2002 during cruise* Poseidon *293*

2 Data

Hydrographic data used in this study were collected at a mooring site in the Central Irminger Sea (CIS, see figure 1.1 on page 2). In addition, Microwave Optimally Interpolated Sea Surface Temperature based on data from the advanced Microwave Scanning Radiometer (AMSR-E) on board the Aqua satellite is added to gaps in the upper 10 to $40\,\mathrm{m}$ of the water column. For determining the oceanic-atmospheric fluxes data from NCEP-Reanalysis-Model (NOAA CLIMATE DIAGNOSTIC CENTER, 2004) are used. Furthermore high-resolution wind data from the SeaWinds microwave scatterometer on the QuikBird satellite (QuikScat) have been analyzed.

2.1 Mooring data

The CIS mooring is an autonomous multidisciplinary time series station located at $59.7°$N $39.7°$W that has been set up in 2002 as part of the EU-FP5 ANIMATE (Atlantic Network of Interdisciplinary moorings and times-series for Europe, *www.soc.soton.ac.uk/animate/*) project. The programme is continued and since 2004 funded by the EU-projects MERSEA (Marine environment and security for the European Area, *www.mersea.eu.org*). The main goal of ANIMATE is to improve the understanding of the interaction between physical and biogeochemical cycling. The mooring is equipped with sensors measuring

- physical parameters (temperature, salinity, pressure and current) from near-surface down to about $1500\,\mathrm{m}$ and

- near-surface biogeochemical parameters of the mixed layer including nitrate, fluorescence and CO2 partial pressure.

Additionally, the mooring is equipped with a satellite link (telemetry). The top buoy sends physical and biogeochemical data in real-time to shore which can be assimilated into numerical models.

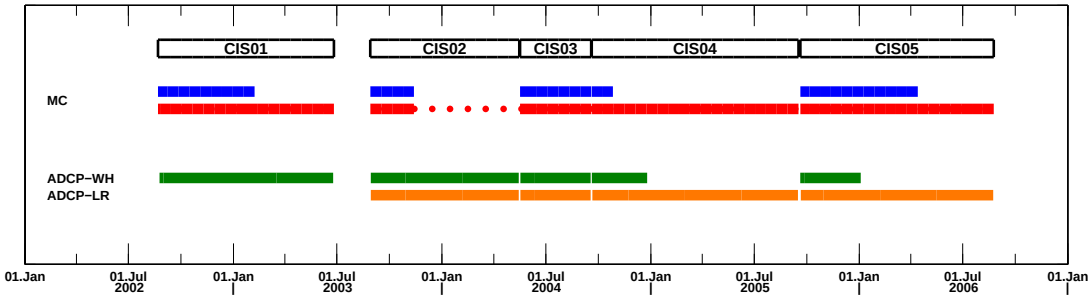

FIGURE 2.1: *Time series of MC- and ADCP-Data availability during all mooring periods from August 2002 to August 2006; blue: full water column, red: water column up to approximately* 50 m *under surface, red dotted line indicates the survival of one instrument that was attached to a second mooring.*

The site is situated in the centre of the Irminger Sea gyre (see figure 1.1), a region of minimum stratification where the maximum depth of convection is expected, and regarding the biological measurements an approximately 1-dimensional system exists that can be interpreted more easily.
Here only physical parameters are considered. SEABIRD MicroCATs (*Micro* Conductivity *A*nd *T*emperature Recorder; hereafter MC) measure temperature and conductivity, and some of them have an additionally pressure sensor. Current profiles are measured acoustically with ADCPs (*A*coustic *D*oppler *C*urrent *P*rofiler). Figure 2.1 shows the availability of these data during all 5 mooring periods. During the first and the second mooring period two moorings have been deployed at the time series site. Since May 2004 all instruments have been attached to one single mooring. Due to damages there are periods where the shallow sensors got lost or even no data were available. The mooring periods are as follows:

- **CIS 1**: 21 August 2002 - 25 June 2003
- **CIS 2**: 28 August 2003 - 15 May 2004
  (1 mooring with 12 MCs failed on 13 November 2003)
- **CIS 3**: 16 May 2004 - 18 September 2004
- **CIS 4**: 18 September 2004 - 16 September 2005
- **CIS 5**: 19 September 2005 - 21 August 2006

Altogether the time series span a period of 4 years with two interruptions of 2 and 6 months.

2.1.1 Temperature and salinity measurements

There have been 11 to 14 MCs attached to the mooring extending from near-surface down to $1000\,\mathrm{m}$ (CIS 1) and $1500\,\mathrm{m}$ (CIS 2 and following) during the deployment periods. During the first two deployments the sampling interval was set to 30 minutes, afterwards the sampling frequency was increased to every 20 minutes. The nominal depth of the instruments used is given in table 2.1, MCs with pressure sensor are marked.

No.	CIS 1	CIS 2	CIS 3	CIS 4	CIS 5
1	10	10	10	10	10
2	37 p	37 p	30 p	20 p	31 p
3	87	85	40 p	38 p	43 p
4	142 p	125 p	70	68	73
5	221	153	109	107	112
6	302	173	155	154	156 p
7	402 p	253 p	197	196	198
8	552	378	267 p	266 p	268
9	702 p	553 p	372	371	373
10	853	754	548 p	546 p	548 p
11	1002 p	1004 p	748	747	749
12	-	1248 p	998 p	993 p	995 p
13	-	1498	1245 p	1244 p	1246 p
14	-	-	1496	1492	1497

TABLE 2.1: *Nominal depth of MCs in* m*. Instruments with pressure sensors are marked.*

The shallowest instrument is at $10\,\mathrm{m}$ depth close to the top buoy to resolve the summerly mixed layer. In 4 out of 5 mooring periods the wire broke and the shallow instrument got lost or left its nominal depth through a break of the top buoy. Therefore sea surface temperatures are added to represent the upper part of the water column. I will get back to this later in section 2.2.1.

The temperature values were calculated according to the practical scale ITS-90. The pressure of the instruments has been corrected by a linear interpolation from the offset at the beginning and at the end of the measurements. Depths of instruments that do not feature a pressure sensor has been calculated by linear vertical interpolation between two instruments with known depths based on the instruments' arrangement in the mooring. After that a pressure correction has been applied to the conductivity cells and the salinity was calculated according to the practical scale PSS-78. As far as time was available during a service cruise a

prior and a post in-situ calibration of the MCs has been carried out by attaching the instruments to a CTD rosette. The data from both instruments are compared. If only one calibration cast was available a bias correction was used, otherwise a linear drift correction was applied to the MC (KARSTENSEN, 2005). If an instrument was used in successive deployments and no calibration cast was done in between a linear drift over the mooring periods has been assumed. The method is also described in more detail by KANZOW (2004). Using this method temperature and salinity measurements reaches an accuracy of $\pm 0.002\,^{\circ}\mathrm{C}$ and ± 0.003, respectively.

Potential temperature (θ) and potential density (σ_0) are derived from the calibrated temperature and salinity. For some of the later presented estimation a gridded data set is used. For that the data have been averaged every day. After that the temperatures and salinities were interpolated using an Akima spline interpolation in the vertical onto a $10\,\mathrm{dbar}$ interval grid. In this case potential temperature and density has been calculated from the interpolated temperature and salinity as well as the gridded pressure.

2.1.2 Current measurements

With the exception of the first deployment period the mooring is equipped with two ADCPs. Both are positioned at a nominal depth of approximately $150\,\mathrm{m}$. Depending on the used frequencies an ADCP can measure vertical current profiles with a range of up to $650\,\mathrm{m}$. One instrument (Workhorse Monitor, $300\,\mathrm{kHz}$) is orientated for measuring upward from near-surface to the instrument depth, the second one (Workhorse Long Ranger, $75\,\mathrm{kHz}$) is directed downward. Some set-up parameters for the instruments during the 4 years of measurements are given in table 2.2 including sampling interval and vertical depth intervals (bin size).

	Workhorse (⇑)			Longranger (⇓)		
	nominal depth	sampling interval	Bin size	nominal depth	sampling interval	Bin size
CIS 1	152m	30min	10m	-	-	-
CIS 2	149m	30min	10m	153m	30min	16m
CIS 3	150m	30min	8m	153m	30min	16m
CIS 4	150m	60min	8m	151m	30min	16m
CIS 5	153m	60min	8m	154m	30min	16m

TABLE 2.2: *Overview of selected set-up parameters of deployed ADCP instruments*

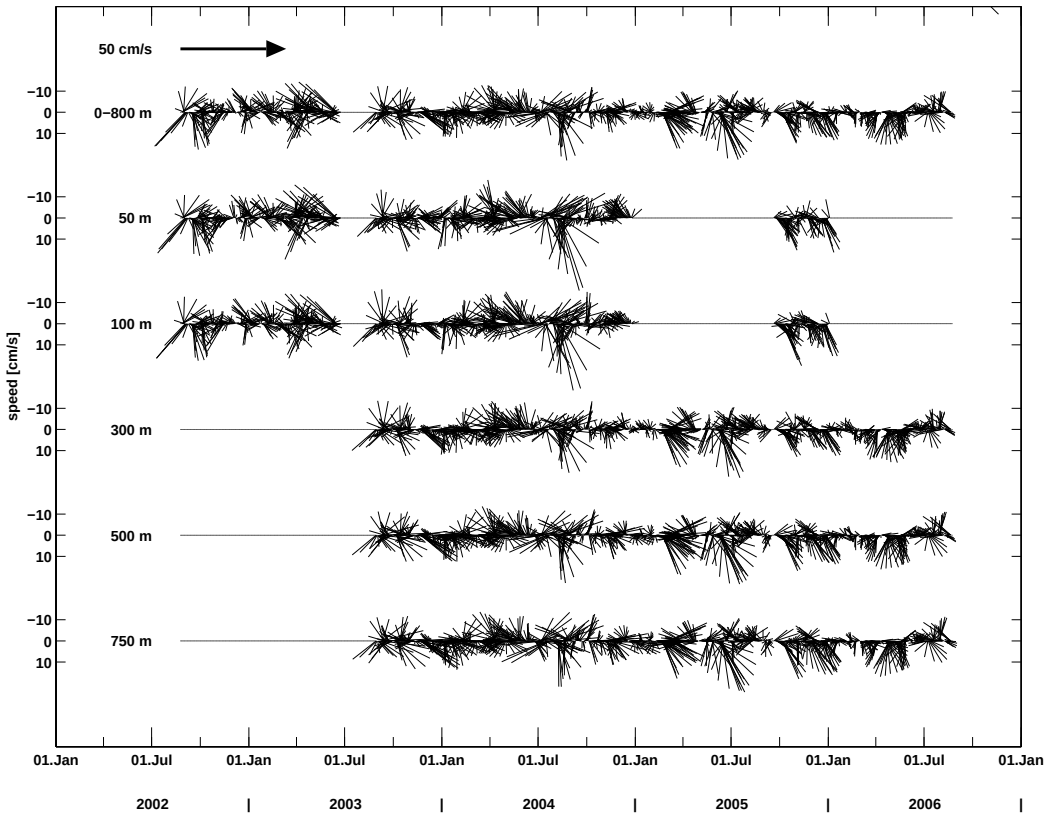

FIGURE 2.2: *Time series of daily current measurements in different depths after passing a* 31*hour low pass filter to suppress tidal signals.*

Intense reflection of the acoustical signal at the boundary layer of atmosphere and ocean disturbs measurements near-surface and data from these bins are neglected. Additionally, there are difficulties to resolve signals close to the instruments. Both instruments together resolve currents of the upper $800\,\mathrm{m}$ of the water column.
During the fourth and fifth deployment the upward looking instrument failed after working for 3 and 6 month, respectively. Availability of continuous recording can be seen in figure 2.1.

Strong barotropic currents can force the mooring to move in the water column during deployment. The variability in depth caused by these movements is corrected by applying pressure variations that are known from the next available MC with pressure sensor.
Figure 2.2 illustrates the 3-day running mean of daily current measurements in different depths. The data passed an 31-hour low pass filter to suppress tidal signals. On top the mean current of the upper $800\,\mathrm{m}$ is plotted. It shows a strong

barotropic component. The signal is furthermore dominated by eddies with periods of some weeks (BEGLER, 2004).
Two additionally mounted rotating current meters at $1000\,\mathrm{m}$ and approx. $2300\,\mathrm{m}$ also reveal a good correlation with the current measured from the deepest bin of the Longranger (not shown here) and emphasizes the barotropic component (RRS DISCOVERY CRUISE REPORT, 2006). Within the 4 years of observation two main flow directions are detectable that change irregularly. About half of the flow is directed west-south-westward with an overall mean velocity of about $7\,\mathrm{cm/s}$ while the other part flows in the opposite direction with an average velocity of about $9\,\mathrm{cm/s}$ leading to a mean shift of $2\,\mathrm{cm/s}$ in east-north-easterly direction.

Both current profiler feature an accuracy of $\pm 0.5\,\mathrm{cm/s}$ and approximately $\pm 1\,^\circ$ in velocity and direction according to information of the manufacturer (RD Instruments).

2.2 Additionally used data

2.2.1 Sea surface data

Sea surface temperature
Temperature data have been filled up with sea surface temperature (SST) to help resolving the summerly shallow mixed layer. The Microwave Optimally Interpolated (MW OI) SST include data from the AMSR-E satellite radiometer provided by RSS (`www.ssmi.com/sst/microwave_oi_sst_browse.html`) and represents the daily minimum SST. The advantages of these data compared to the SST products NCEP OI and NOAA RTG are daily values with a horizontal resolution of $\sim\ 25\,\mathrm{km}$, and due to the frequency, the possibility of measuring through clouds. Extensive comparisons of MW OI SSTs to NCEP OI (Reynolds) SSTs performed by RSS reveals a bias of $-0.02\,^\circ\mathrm{C}$ and a standard deviation of $0.64\,^\circ\mathrm{C}$ for the global collocation. Differences are expected, as the MW OI SST resolve real SST features that are smoothed out of the low resolution NCEP OI SSTs (REMOTE SENSING SYSTEMS, 2006a).

These differences can also be seen in figure 2.3 (top) that shows the weekly sea surface temperature of both OI SST products for grid points close to the mooring site and for comparison the temperature of the shallowest MC. Summerly SST from the instrument attached just beneath the top buoy shows a high correlation with the satellite data. Especially during wintertime the SST collected from AMSRE better fits with the data from the mooring site. The panels below show histograms of the difference between SST and near-surface temperature measured by the mooring. The left panels show values for the instrument close to the top

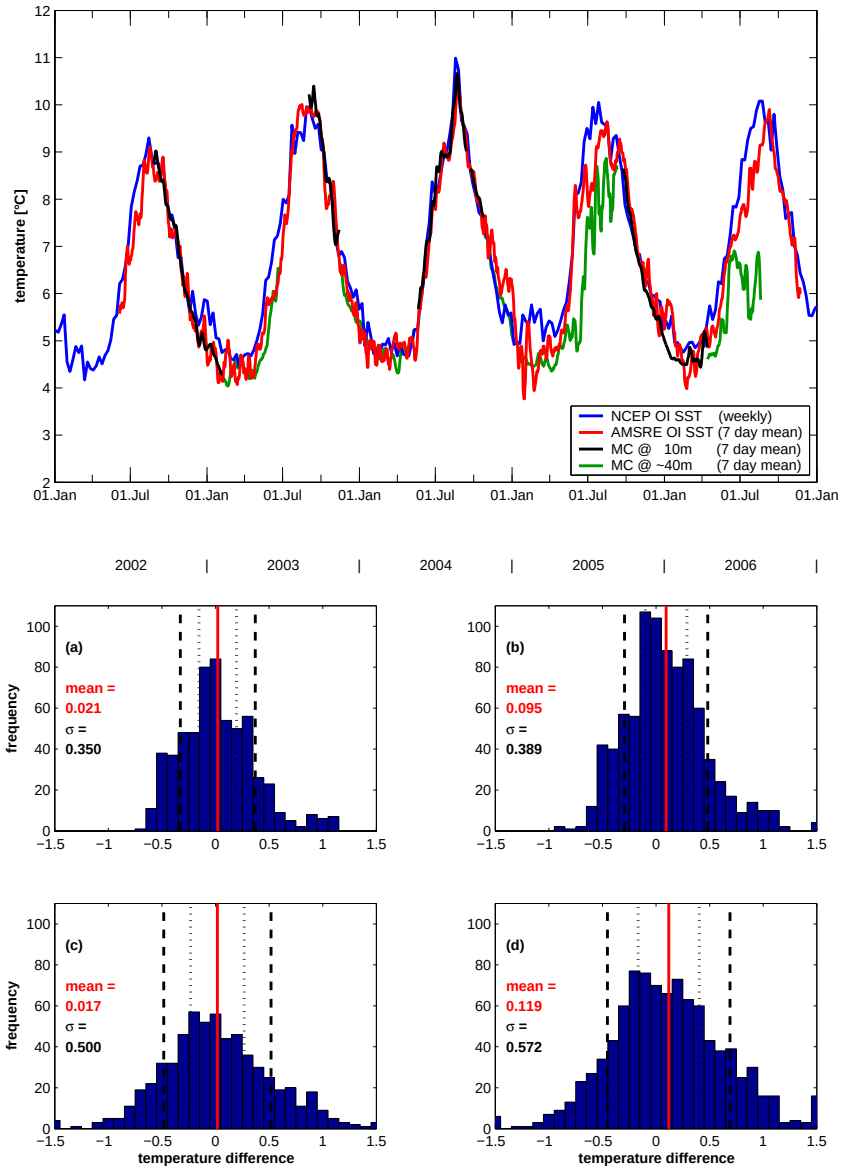

FIGURE 2.3: *Comparison of weekly mean sea surface temperatures and near-surface temperature of shallow MCs. The blue line represents the NOAA OI SST data for a grid point close to the mooring, while the red line shows the weekly mean OI SST derived from AMSR-E. Subsurface data at about* $10\,\mathrm{m}$ *(magenta) and* $40\,\mathrm{m}$ *(cyan) nominal depth are also displayed.*
Below: histograms of difference between SST and temperature of shallow MC. Panel ***(a)****: weekly mean, near-surface instrument;* ***(b)****: weekly mean, maximum instrument depth is* $40\,\mathrm{dbar}$*;* ***(c)****: daily data, near-surface instrument;* ***(d)****: daily data, maximum instrument depth is* $40\,\mathrm{dbar}$*. Vertical lines indicate the mean value (red) and standard deviation that represent the* σ*- (dotted) and* 2σ*- (dashed) area.*

buoy for daily data (a) and weekly mean values (c). Panel (b) and (d) display the same for data from the shallowest available instrument with a maximal pressure of $40\,\mathrm{dbar}$. This means after loosing the top instruments, data from the MC at $40\,\mathrm{m}$ nominal depth are taken into account in addition. Times when strong currents caused a subduction of the mooring beneath this depth are neglected. Even in the worst case the correlation between the MC data and the SST over all the mooring periods is higher than 0.94. On average the temperature of the SST is less than $0.12\,^{\circ}\mathrm{C}$ higher compared to the MC in all four cases which makes sense as the MC is deeper, thus colder. The comparison with the instrument at $10\,\mathrm{m}$ even shows a difference of $0.02\,^{\circ}\mathrm{C}$ on average. The mean value and standard deviation are also plotted in the graphic. Approximately 41% and 70% of the data lie within the σ- and 2σ-area, respectively. This reveals that the SST is a satisfying representation of the upper 10 to $40\,\mathrm{m}$ of the water column.

Sea surface salinity
Sea surface salinity (SSS) has been constructed by using the linearised density equation:

$$\rho = \rho_0 \left[1 - \alpha_\theta (T - T_0) + \beta_S (S - S_0)\right] \tag{2.1}$$

where α_θ and β_S are thermal expansion and haline contraction coefficients, respectively, and T_0 and S_0 are reference temperature and salinities (e.g. **?**).
By forcing the surface to have the same density as the shallowest MC the equation simplifies to:

$$SSS = S_0 + \frac{\alpha_\theta}{\beta_S}(SST - T_0) \tag{2.2}$$

whereas T_0 and S_0 are given by the instrument. In summertime when the upper MC was not available the instruments' density was firstly compared with World Ocean Atlas 2001 climatology (NOAA NATIONAL CLIMATE LABORATORY, 2004). If the difference was higher than $0.24\,\mathrm{kg/m^3}$ data were neglected. In these cases the linearised density equation would not have been a good approximation. For further validation the surface density has been evaluated by using the SST and constructed SSS and compared to the density of the shallowest instrument. The result is given in figure 2.4. At the top the salinity measured by the shallowest MC and data that are constructed using the SST can be seen. The salinity maximum in summer 2005 seems suspicious. But it is not completely absurd. A CTD profile generated in September 2005 close to the mooring site also featured a salinity maximum of 35.1 at $60\,\mathrm{m}$ depth. Thus, an event yielding to relative high salinity may have taken place during this period.

To prove the correctness of the linearity presumed in Eq. (2.1), the density at surface has been derived from the SST and SSS. The result is displayed in the panel below and shows a good agreement with the density of the shallow instru-

ment as originally forced. A comparison with the also plotted climatology reveals an underestimation of density during November to January by the climatology. According to the construction of the sea surface salinity this had no impact.

The daily mean sea surface temperature and salinity have been added to the moorings' data set and taken into account for vertical interpolation as already mentioned on page 10.

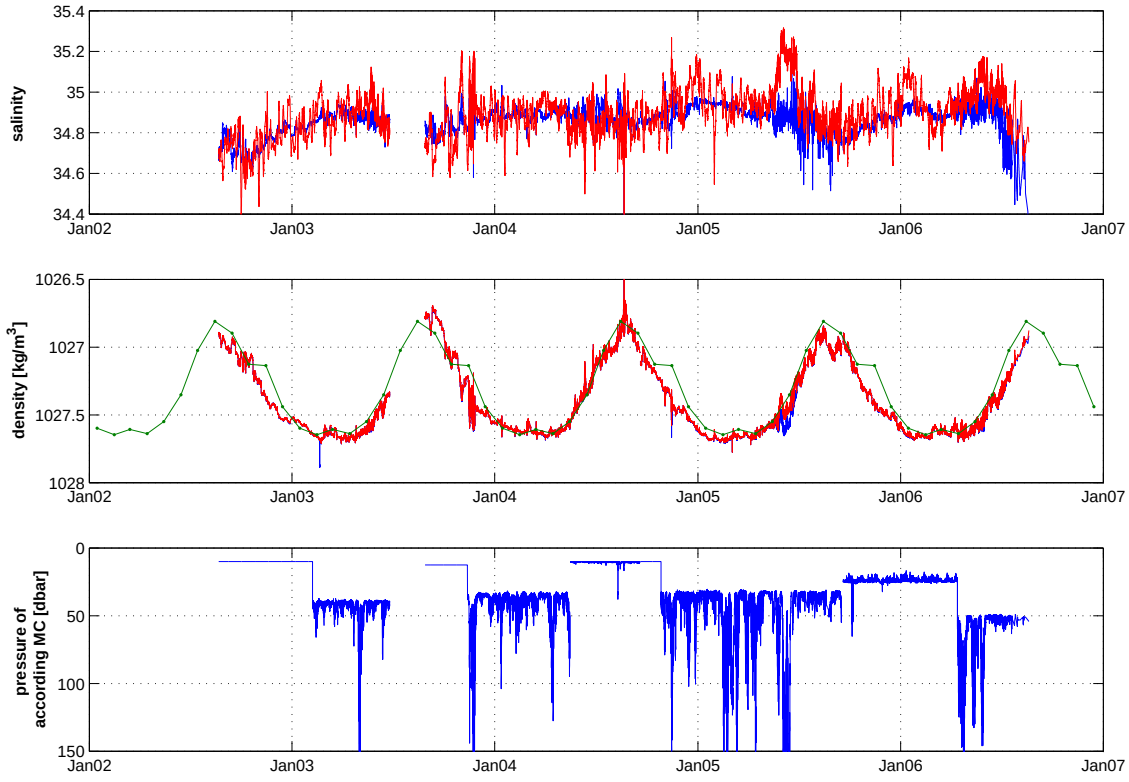

FIGURE 2.4: *First Panel shows the salinity of the shallowest MC (blue) and constructed surface data (red). In the middle time series of density are presented. Green indicates data from the climatology for this area, data from the shallowest MC and from surface derived from SST and constructed SSS are plotted; colours as above. The panel below illustrates the pressure of the shallowest available instrument that is used for calculating the SSS.*

2.2.2 NCEP-Reanalysis surface heat fluxes

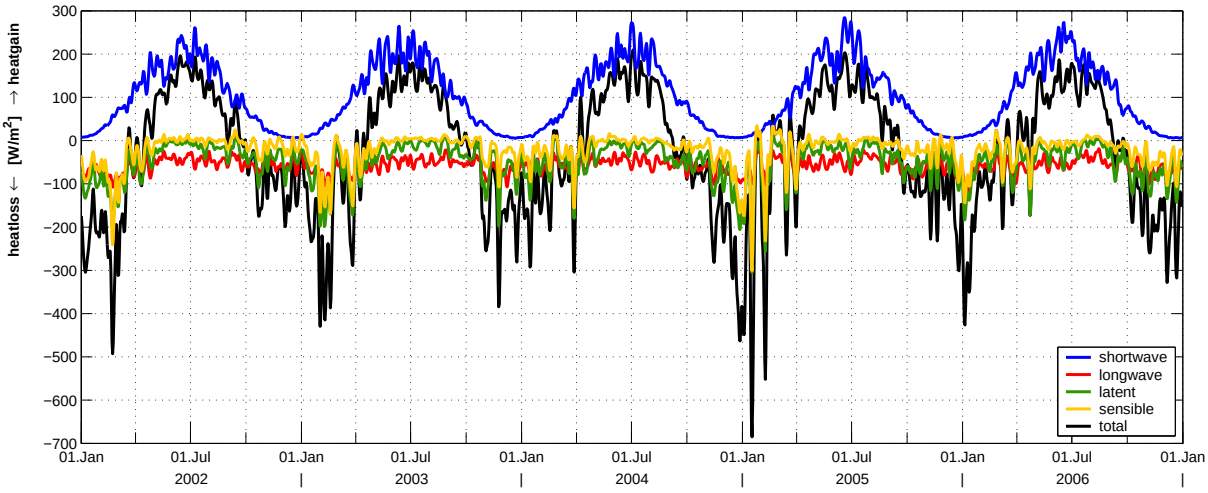

FIGURE 2.5: *Time series of daily NCEP/NCAR model heat flux components averaged over 7 days for a grid point close to the mooring over the time period Jan 2002 - Dec 2006.*

Observation of meteorological data at sea is rare over the open ocean. Therefore, NCEP Reanalysis data are used to estimate the atmospheric conditions of the mooring site. Reanalyses are combining atmospheric model data and observation that are used to minimize model errors. In this study NCEP daily mean surface heat fluxes with a horizontal resolution of $1\,^\circ \times 1\,^\circ$ are used.
Errors in the NCEP/NCAR Reanalysis data are not provided but uncertainties are expected. Surface heat fluxes are not directly measured and strongly depend on the quality of the underlying model and its parametrisation. RENFREW ET AL. (1994) compared surface flux observations over the winterly Labrador Sea collected by ship measurements with NCEP Reanalyses and estimated errors of some $10\,\mathrm{W/m^2}$ for latent and up to $100\,\mathrm{W/m^2}$ for sensible heat flux. Or in other words, the NCEP model overestimated the heat fluxes by 27% and 51%, respectively. Another comparison based on global vessel observations (SMITH ET AL., 2001) also revealed an overestimation of the turbulent heat fluxes by the NCEP model. But the bias error is just of about $10\,\mathrm{W/m^2}$ (latent) and $5\,\mathrm{W/m^2}$ (sensible) for data collected between $50\,^\circ$ and $70\,^\circ\,\mathrm{N}$. The time series of the heat flux components for the grid point $60°\mathrm{N}\ 39.37°\mathrm{W}$ that is closest to the mooring is illustrated in figure 2.5 for the time period January 2002 to December 2006. Positive values are associated with heat gain by the ocean. Displayed are 7-day averages of daily model data. During winter 2004/2005, where highest heat loss is obtained, individual daily values even exceeds a loss of over $1000\,\mathrm{W/m^2}$.

2.2.3 Wind Data

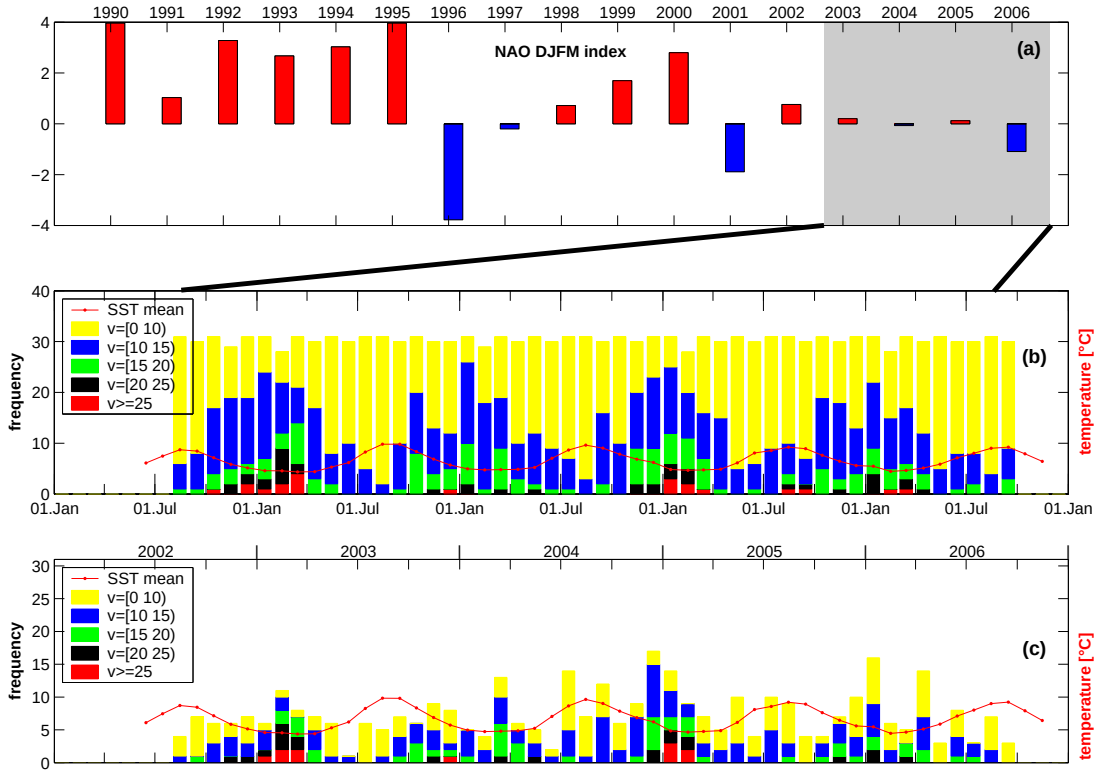

FIGURE 2.6: *Panel **(a)**: time series of DJFM NAO index for the last* 16 *years, mooring period shaded. Panel **(b)** and **(c)**: Monthly frequency of daily wind speed [m/s] to all directions and directions deviating at most* 30 ° *from east,respectively.*

As mentioned earlier the NCEP reanalysis does not properly resolve the Greenland tip jet due to its low resolution and may underestimate the turbulent heat fluxes. But the influence of this wind pattern that can enhance the surface heat fluxes and lead to more intense cooling is not negligible. Comparing results of a 1-D model driven by original NCEP fluxes and fluxes that has been modified by taking QuikScat wind data into account showed the influence of the Greenland tip jet on the deepening of the mixed layer depth in the Irminger Sea (VÅGE ET AL., 2006). Greenland tip jets occur more often during times of a high winter NAO index. This can also be seen in figure 2.6 for the mooring time period, a time of rather low NAO index compared to the beginning and mid of the 1990's. In this study the original NCEP fluxes are used for estimating the development of heat fluxes on the mooring site. Daily averaged QuikScat wind data are taken into account for evaluating the development of the mixed layer depth. They

are measured twice every day depending on the swath and have a horizontal resolution of $\sim 25\,\mathrm{km}$. Tip jet events are referred to wind events with speeds greater than $20\,\mathrm{m/s}$ and directions with a maximum deviation of $30\,^\circ$ from east as suggested by VÅGE ET AL. (2007). Most tip jet events occurred in winter 2002/2003 followed by winter 2004/2005. During the latter, all events happened in a period between end of December to mid of February while in the first winter the events took place more scattered during mid of November and end of March. In winter 2003/2004 and winter 2005/2006 which is associated with a more negative NAO index only less than 5 strong scattered tip jet events are recognizable. According to the utterance of VÅGE ET AL. (2006) this might lead to the conclusion that during the last winter the mixed layer depth would be less well developed than during the winters before. Actually this is not found here as it will be shown later in chap 3.2 (see table 3.1).

3 Results

The aim of this chapter is the estimation of the heat and freshwater fluxes in the Central Irminger Sea. At first, different ways to estimate the mixed layer depths (MLD) are briefly compared. This is followed by an analysis of the hydrographic parameters.

3.1 Estimating the mixed layer depth

In general, the ocean mixed layer is considered to be the near-surface quasi-homogenous region of the upper ocean where the oceanic properties (temperature, salinity and density) show just little variations in the vertical, followed by a layer with more rapid changes. The vertical uniformity of the layer is caused by intense vertical turbulent mixing. The vigorous turbulence is generated by the action of wind stress and vertical buoyancy fluxes at the ocean's surface.

Time series of the oceanic properties for different instruments at given nominal depths are shown in figure 3.1. The homogenization of the upper $150\,\mathrm{m}$ starts in December each year when the near-surface temperatures lower down to $5\,^{\circ}\mathrm{C}$ and less. The all year record of instruments attached at $\sim 150\,\mathrm{m}$ show an annual cycle with a slow increase in temperature and salinity during the non-convecting part of the year which is followed by a rapid decrease during winter time. The density shows an opposite development. The time for convective activity is strongly restricted. Depending on the initial state of the water column at the end of the precedent summer the deepening of the MLD beneath $150\,\mathrm{m}$ appears between mid of December and end of January in the following year. The restratification already starts in March when the intensity of the surface heat flux and frequency of strong turbulence inducing wind events diminishes. Thus, the time for establishing a deep MLD is limited to the period between January and February. Nevertheless, it is obviously that the homogenization did not reach the instruments that are attached to the mooring below $700\,\mathrm{m}$ during all deployment periods.

The deepest MLD can be found in winter 2005, the time with the most intense surface heat fluxes, considerably weak mean current and several strong wind events occurring in short temporal sequence (see figure 2.5, 2.2 and 2.6). In December 2002 the temperature already shows a rather uniform structure. But the presence

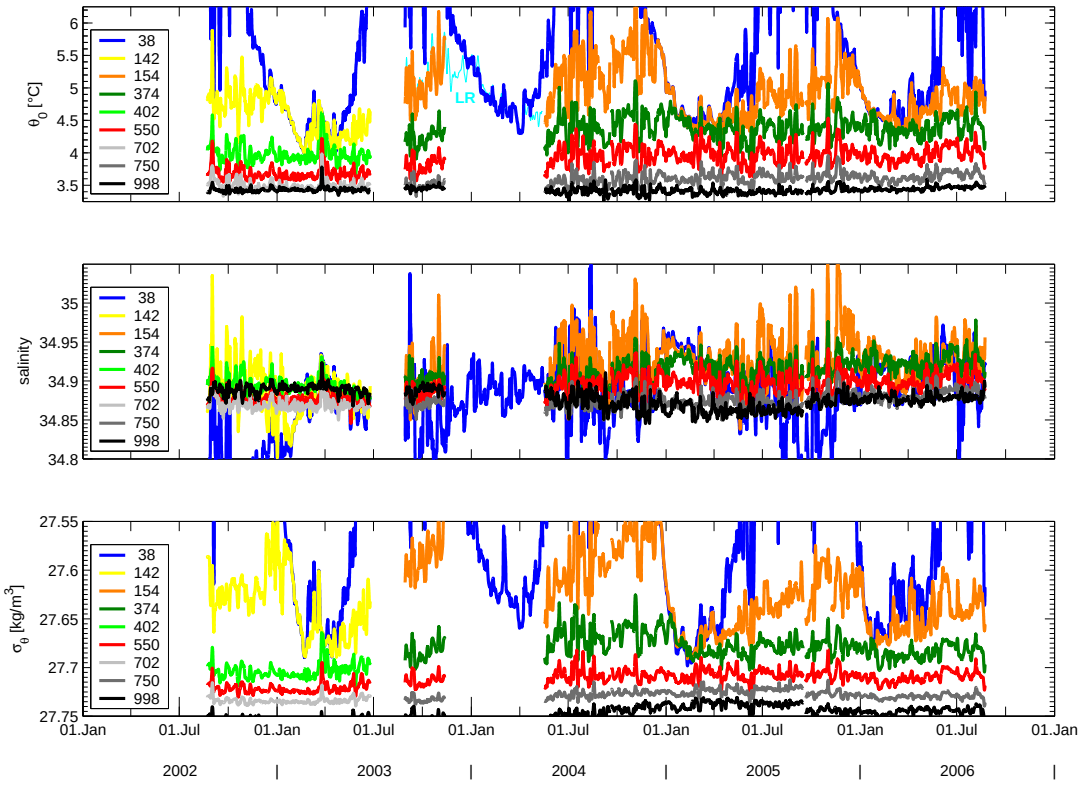

FIGURE 3.1: *Time series of potential temperature (top), salinity (middle) and potential density (bottom) as measured by instruments* $1000\,\mathrm{m}$ *deep and shallower. Records have been lowpassed using a 48-h Hanning filter to eliminate periods shorter than 1 day. LR indicates uncalibrated temperature measured by the downward looking ADCP.*

of relatively fresh water suppressed the beginning of the mixed layer deepening. It took about one month to homogenize the layer down to $140\,\mathrm{m}$ nominal depth. Within this time the temperature decreased by approximately $\sim 0.5\,^{\circ}\mathrm{C}$. For the winter period 2003/2004 no data are available because of mooring loss. But a comparison of the temperature recorded by a remaining instrument at about $40\,\mathrm{m}$ with the uncalibrated temperature measured by the ADCP Longranger (indicated by "LR" in fig. 3.1) in $\sim 150\,\mathrm{m}$ depth reveals that the mixed layer was deeper than $150\,\mathrm{m}$ between late December 2003 and early April 2004. Winter 2006 has the lowest NAO index for the whole mooring period, and especially in February the net surface heat flux is lower than during the other years. Nevertheless for a short time in January a homogenization down to $\sim 400\,\mathrm{m}$ can be found. But as it will be shown later, the density of this mixed layer is much lower than during winter 2002/2003 and winter 2004/2005.

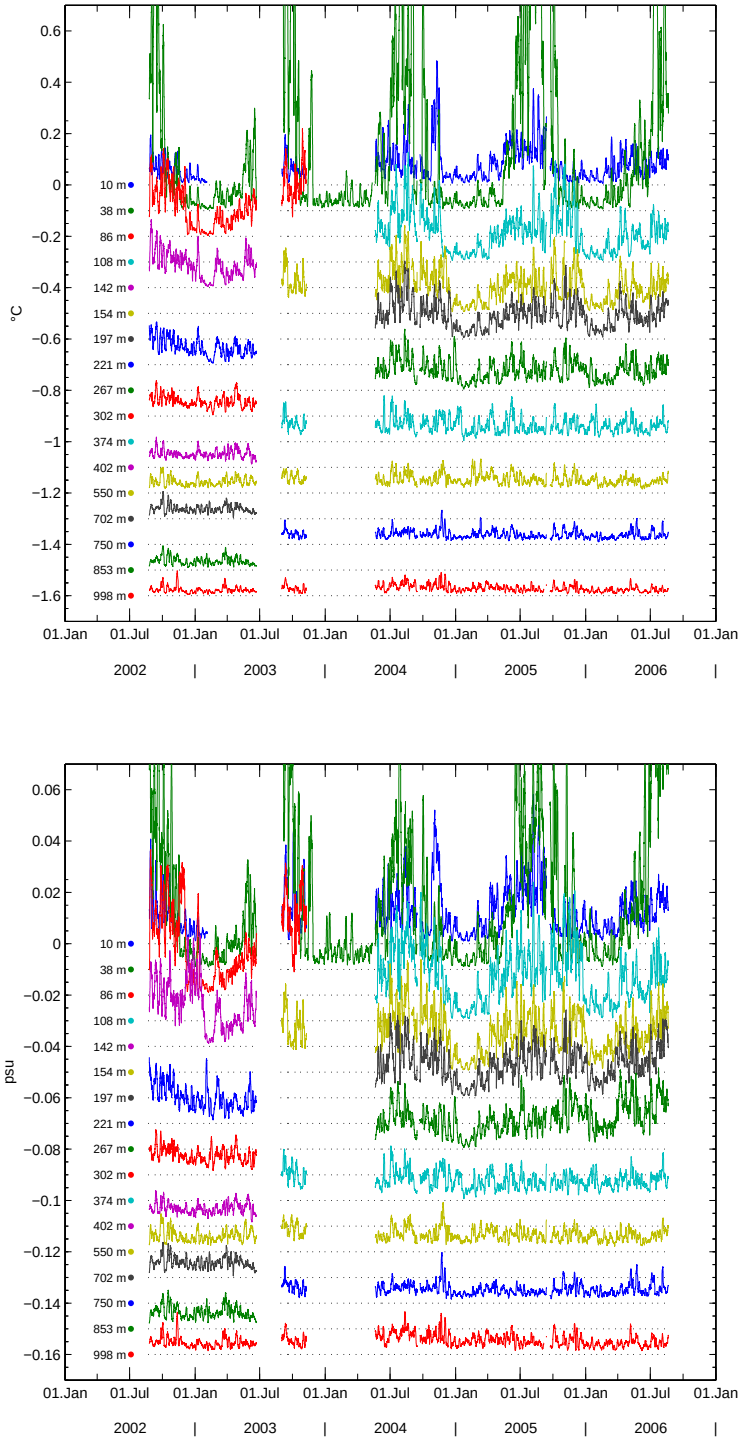

FIGURE 3.2: *Moving standard deviation of high frequency θ (top) and salinity (bottom) fluctuations at different instrument depths. First time series are lowpassed with a 96-h-Hanning filter, afterwards removed from the original data. Due to noisiness standard deviation over 3 days was determined and is displayed.*

A different way in estimating the MLD from moored instruments is based on the reduction of high-frequency variability in the temperature and salinity time series. The time series of temperature and salinity that has been high-pass filtered (96-h filter width) show a high variability for both parameters throughout the year. The signal is extremely noisy. This large day-to-day variability at short time scales can be interpreted as the result of lateral fluxes and variations in the density field, e.g. due to internal waves. The amplitude of the fluctuations is typically $\sim 0.3\,^{\circ}\mathrm{C}$ in potential temperature and ~ 0.04 in salinity for instruments between 300 and $800\,\mathrm{m}$, for shallower instruments occasionally two times higher. In wintertime a remarkable decrease in fluctuation is visible. Due to the noisiness the moving standard deviation over 3 days for the high-frequency fluctuations at different given instrument depths was calculated and is displayed in figure 3.2. And even here it is difficult to detect the times of mixed layer deepening. Just for instruments shallower than $400\,\mathrm{m}$ a temporal minimum after increased variability can be found. Highest variability shows the instrument at $\sim 40\,\mathrm{m}$ depth during summertime as it often passes in and out of the shallow summerly mixed layer due to internal wave heave and mooring movements with vertical excursions of $50\,\mathrm{m}$ or even more.

The analysis of the data so far just leads to a rough estimation of the MLD as the real position of the sensors due to mooring movements are not yet taken into account. To take these movements into consideration the gridded data set of the oceanic parameters is used from now to calculate the development of the MLD.
There are several concepts to estimate the oceans' MLD. Many of them use a Δ-criteria. In these cases the MLD is defined as the depth where the temperature decreased or potential density increased by a constant value Δ compared to a reference value, commonly the surface. A list of various published Δ-criteria can be found for example in the publication of KARA ET AL. (2000). Some of them are applied to the data set and illustrated in figure 3.3 on top of contoured graphics of potential temperature θ_0, salinity, potential density σ_0 and buoyancy frequency N^2 for the upper $1000\,\mathrm{m}$ of the water column. MLD derived from using a temperature decrease of $0.5\,^{\circ}\mathrm{C}$ ($1.0\,^{\circ}\mathrm{C}$) is illustrated by the bold (thin) dashed line. Furthermore, a density change due to a temperature decrease of $0.8\,^{\circ}\mathrm{C}$ as suggested by KARA ET AL. (2000) is indicated by the thin solid line. It is obvious that all these 3 criteria overestimate the actually existing mixed layer. Among them the Δ-θ criterion of $0.5\,^{\circ}\mathrm{C}$ seems to be the best estimation, but it still underestimates the influence of salinity which can be seen for instance in late winter each year.
A freely chosen density difference of $0.015\,\mathrm{kg/m^3}$ relative to surface better represents the MLD (bold solid line in figure 3.3). The fluid of the layer shows relatively homogenous salinity and temperature properties. Additionally, this estimation follows the upper margin of high buoyancy frequency, which represents the

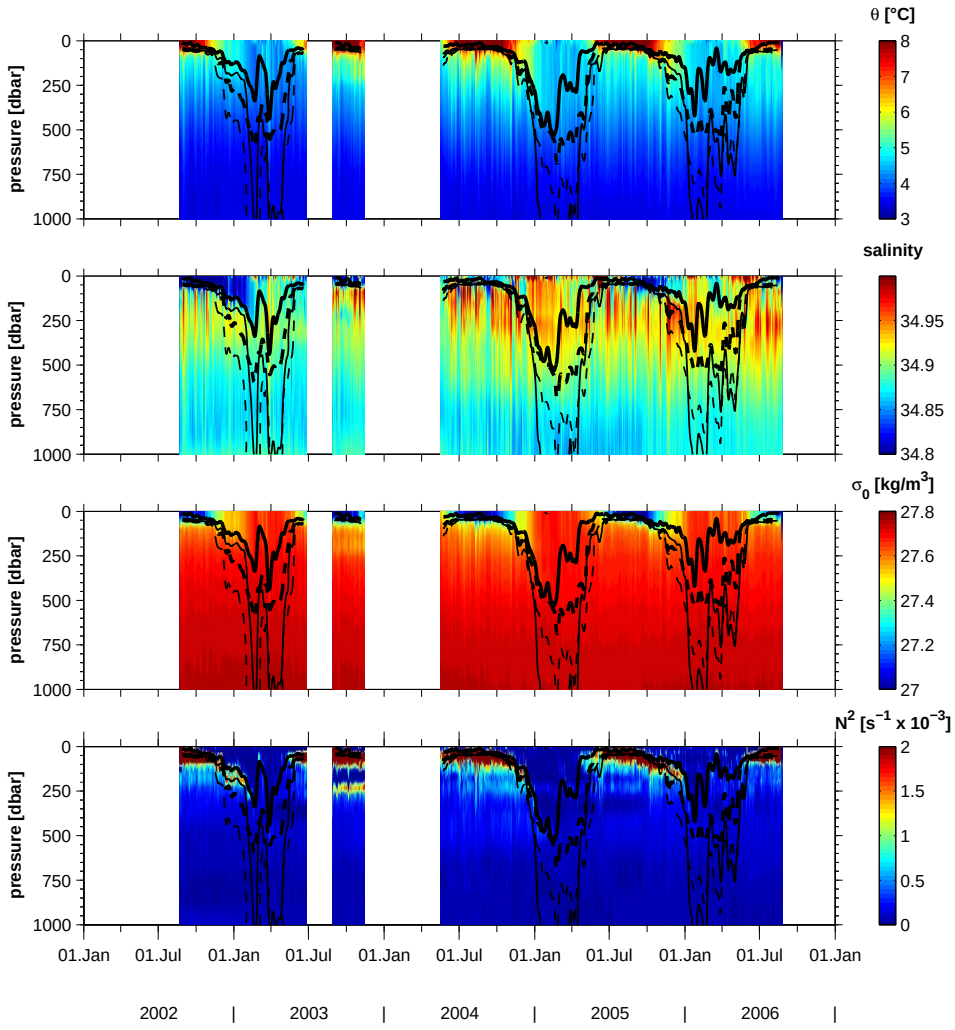

FIGURE 3.3: *Time series of daily potential temperature θ_0, salinity, potential density σ_0 and buoyancy frequency N^2 (from top to bottom).*
Lines indicate MLD estimations after being lowpassed over 7 days. MLD using a temperature change of $0.5\,^{\circ}\mathrm{C}$ and $1\,^{\circ}\mathrm{C}$ relative to surface are given by the bold and thin dashed lines, respectively. The thin solid line represents a density increase associated with a temperature decrease of $0.8\,^{\circ}\mathrm{C}$. The MLD derived by an ad hoc chosen density difference of $0.015\,\mathrm{kg/m^3}$ is indicated by the bold solid line.

rapidly changing density and thus the maximum extent of the mixed layer. During wintertime the signal vanishes more and more and makes the identification of a strong stratified layer more difficult, but it can still be detected (not shown here). Therefore the MLD is determined by using the density difference $0.015\,\mathrm{kg/m^3}$.

3.2 Development of physical properties

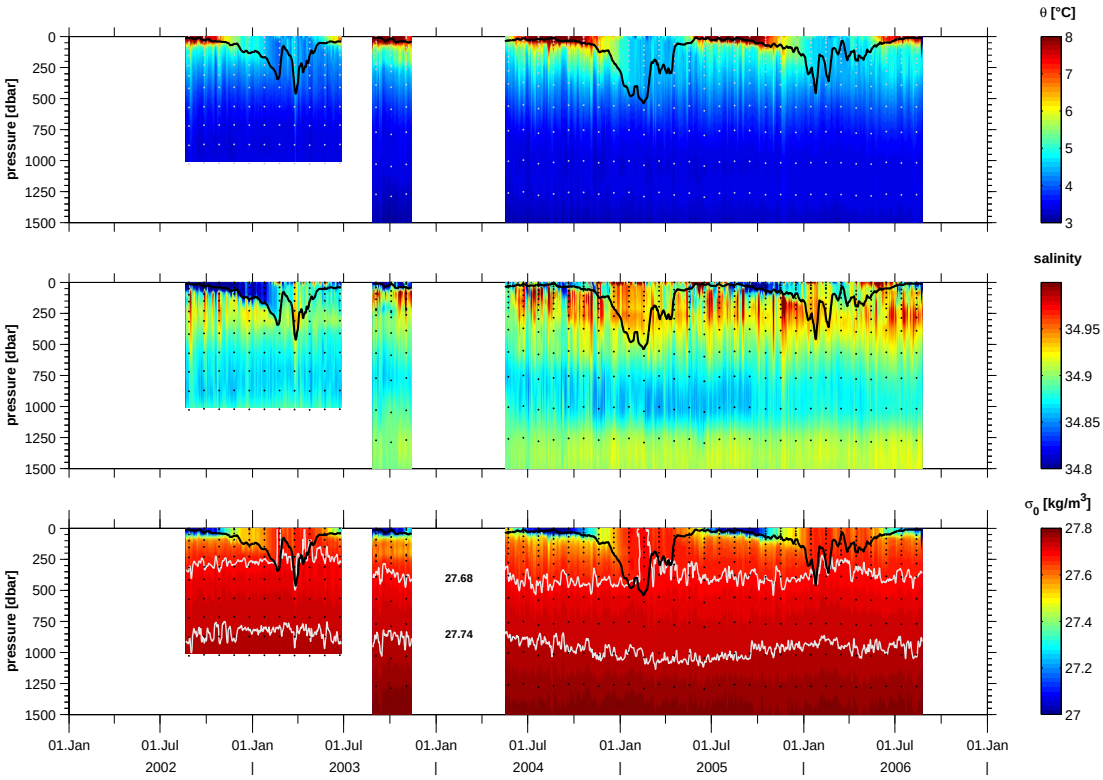

FIGURE 3.4: *Time series of potential temperature (top), salinity (middle) and potential density (bottom). Black and white dots denote the instruments' depth every 30 days. The mixed layer depth is indicated by the black line, smoothed over 7 days. Isopycnals of* $\sigma_0 = 27.68 kg/m^3$ *and* $\sigma_0 = 27.74 kg/m^3$ *are labeled and marked with gray lines.*

The time series of the temporal and vertical equally gridded properties are contoured for the upper $1500\,\mathrm{m}$ (figure 3.4). This covers the range of the maximum established mixed layer depth during all mooring periods. Furthermore, the upper LSW (uLSW), indicated by a salinity minimum at approximately $800\,\mathrm{m}$, can be seen. Due to instruments loss a gap of 6 months occurred that includes winter 2003/2004. Nevertheless, over the observed period a warming trend together with an increase of salinity is visible for the whole water column. The properties show an obvious variability on seasonal and shorter time scales. Warm core eddies pass the mooring irregularly and lead to strongly varying temperature and salinity signals down to $500\,\mathrm{m}$. These temporally varying saline, warm events appear more often during summer and autumn.
Temperature and salinity are rather uniform within the mixed layer which is extent is determined by using the above-mentioned MLD criterion. Deepest

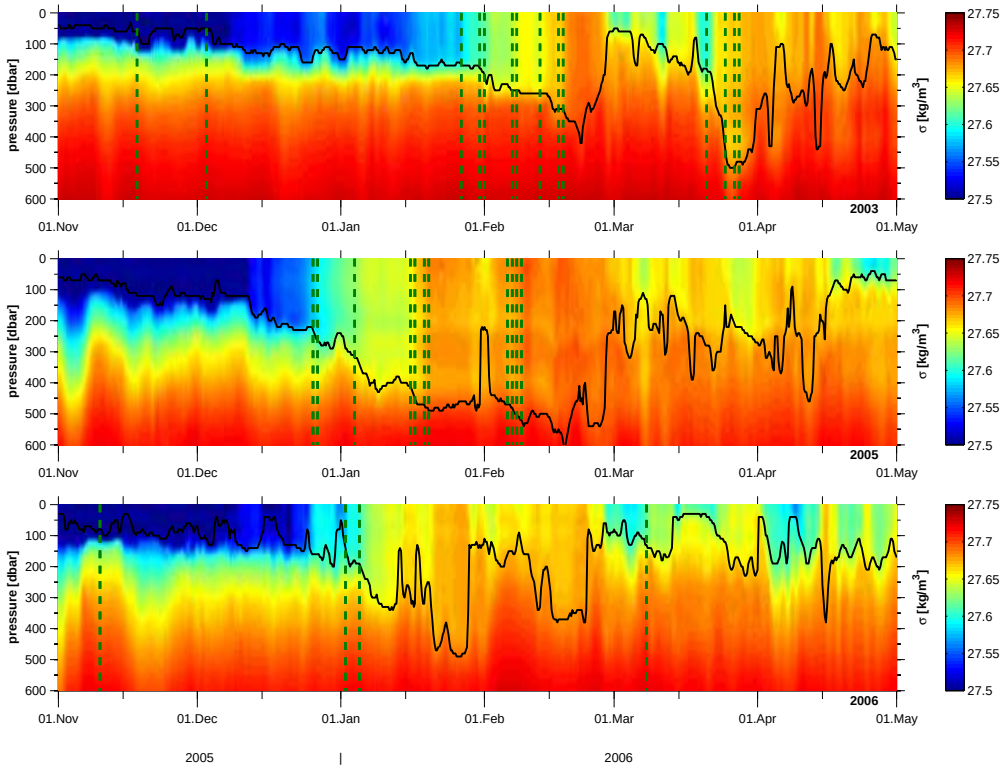

FIGURE 3.5: *Time series of potential density for the 3 recorded winters (top: 2002/2003, middle: 2004/2005, bottom: 2005/2006). The daily mixed layer depth is indicated by the black line. Vertical dashed lines denote days with wind speeds greater than* $20\,\mathrm{m/s}$ *and directions with a maximum deviation of* $30\,^{\circ}$ *from east.*

mixed layer occur in late January and February each year. As already mentioned, restratification starts in early March again. Occasionally, a second deep-reaching mixed layer can be seen in late March / beginning of April. But at this time the density of the mixed layer has decreased. The maximum mixed layer depth does not exceed $700\,\mathrm{m}$. Thus, the uLSW layer is not ventilated at the CIS mooring site during observed period.

At intermediate depth of about $800\,\mathrm{m}$ the potential temperature shows an almost constant increase of $\sim 0.07\,^{\circ}\mathrm{C\,yr^{-1}}$, interrupted by a temporary minimum in late winter 2006. In contrast to this the salinity just slightly increased by ~ 0.001 (which is less than the estimated error for the measurements) between summer 2002 and summer 2005, leading to a steady decrease of the potential density. During the last year an abrupt salinity increase of ~ 0.015 followed that shows the same temporary minimum in 2006. This large increase partly compensates the so far decrease of potential density in this depth. The level of the isopycnals also

illustrates this development (figure 3.4, bottom). The isoline of $\sigma_0 = 27.74\,\mathrm{kg/m^3}$ is shallowest in winter 2002 at about $800\,\mathrm{m}$, deepens down to $1100\,\mathrm{m}$ within 3 years and gets shallower again within 6 months until it ends up at a depth of approximately $950\,\mathrm{m}$.

Since the second deployment the measurements are extended to $1500\,\mathrm{m}$. This deep record shows the development of the upper margin of the lower LSW (lLSW). The evolution for the temperature is comparable to that found in intermediate depths. The salinity in this depth increased by ~ 0.017 within the last 3 years, whereas the value remained almost stable between November 2004 and October 2005. These changes in both depth levels are likely a result of lateral fluxes of heat and salt from the surrounding. In part the changes may be attributed to the changed properties of the LSW itself (AVSIC ET AL., 2001).

At shallower depth the record shows an increase of the winterly temperature in the upper $400\,\mathrm{m}$. This can also be seen in the development of the SST (figure 2.3, top panel, page 13). The maximum summerly and winterly SST in the first year were lower than in the following seasons. On the other hand, autumn 2002 is dominated by a fresh water anomaly. This led to a well established mixed layer of relatively low density in December 2002 that persisted about 1 month longer than in the other recorded winter and made the deepening of the mixed layer more difficult (figure 3.5, top panel). In other words the preconditioning of the water column in the first recorded winter may have suppressed deeper convection.

A comparison of observed mixed layer properties and depths for each winter is given in table 3.1. It also lists the properties and observed convection depths in the Labrador Sea for the time of LSW formation in different years. Winterly maximum mixed layers in the Irminger Sea is by far shallower than observed convection depths in the Labrador Sea. The mixed layer is about $1\,^{\circ}\mathrm{C}$ warmer and 0.04 to $0.08\,\mathrm{psu}$ more saline than the LSW at its formation time. Thus, even the densest fluid found in the Irminger Sea at the mooring site is still lighter than the water formed in winter in the Labrador Sea.

During the first winter, MLD in the Irminger Sea reaches a maximum of approximately $350\,\mathrm{m}$; single days show an extension down to $400\,\mathrm{m}$. Although several tip jet events took place in February that led to enhanced heat flux and stirring, a further deepening could not be achieved due to the stronger stratification. According to figure 3.5 (top panel) the most intense deepening just happened at the time of the tip jet events. This may lead to the assumption that during a comparable winter that starts with a better preconditioned water column, a deeper MLD could have been established, e.g. as observed in winter 2004/2005.

A second MLD maximum occurred end of March, but at this time the water of the layer is less dense, as it is almost $0.5\,^{\circ}\mathrm{C}$ warmer and just slightly more saline ($\sim 0.05\,\mathrm{psu}$). On the one hand this deepening may again be due to the occurrence of strong wind pattern. But on the other hand the water column shows an increase in temperature and salinity down to $\sim 800\,\mathrm{m}$ and is caused at least in part by the presence of a warm core eddy that passes the mooring site.
Deepest MLD appeared in February 2005. This winter shows a well-established and almost constant mixed layer of $500\,\mathrm{m}$ on average that persisted for several weeks. Single days even exceeded a depth of $600\,\mathrm{m}$. The winter started with a rather well preconditioned water column in respect to salinity. Furthermore, the velocity of the mean current as well as its monthly fluctuations was extremely low in January. Thus, for about one month the same body of water was exposed to several occurring tip jet events and to the most intense surface heat flux during

	Labrador Sea [a]				Central Irminger Sea			
Year	Convection Depth	θ LSW	salinity LSW	σ_0 LSW	MLD	θ	salinity	σ_0
1995	2300	2.68 $\pm$0.05	34.82_3 $\pm$ 0.01	27.78_1 $\pm$0.008				
2001	1100	3.16 $\pm$0.07	34.82_1 $\pm$0.021	27.73_7 $\pm$0.010				
2002	1200	3.22 $\pm$0.11	34.83_5 $\pm$0.024	27.74_1 $\pm$0.009				
2003	1400	3.22 $\pm$0.08	34.83_7 $\pm$0.017	27.74_0 $\pm$0.006	350 *450* [b]	4.08 $\pm$0.07 *4.55* *$\pm$0.13*	34.87_8 $\pm$0.013 *34.92_6* *$\pm$0.011*	27.68_1 $\pm$0.009 *27.66_9* *$\pm$0.007*
2004	700							
2005	1300	3.42 $\pm$0.07	34.85_7 $\pm$0.006	27.72_9 $\pm$0.002	500	4.46 $\pm$0.09	34.93_3 $\pm$0.007	27.68_4 $\pm$0.007
2006					400	4.58 $\pm$0.07	34.93_3 $\pm$0.014	27.67_0 $\pm$0.007

TABLE 3.1: *Mean water properties within the water column for the Labrador and Central Irminger Seas. For the Labrador Sea the data are averaged from 400 m to the convection depth and represent the properties during LSW formation time end of March. The values for the Irminger Sea are averaged from 100 m to the mixed layer depth.*
[a] data adopted from AVSIC ET AL. (2001)
[b] properties of second observed deep mixed layer

the four observed winters (see figure 2.5) and experienced persistent heat loss. Although the water column at the end of 2005 looks nearly like at the end of 2004 the finally established MLD in winter 2005/2006 is comparable to that observed during the first winter. Additionally, it persisted just a few days and strongly varied between 200 and $400\,\mathrm{m}$. The water properties are similar to those observed at the second MLD maximum in winter 2003. That such deep MLD could be observed, despite less surface heat fluxes, may be caused by the low velocity of the mean current. Due to this the same fluid body stayed in the area comparable to January 2005.

The observed MLD of the first and third winter are comparable with results that were derived from the other two mentioned mooring arrays in this area. An observation of the Dutch LOCO-mooring (indicated by yellow dots in figure 1.1) showed an increase in MLD to over $600\,\mathrm{m}$ in a few days during winter 2004/2005 (DE JONG AND VAN AKEN, 2006). Regarding data that were collected by a moored profiler from WHOI (green dot in figure 1.1) the MLD reached $400\,\mathrm{m}$ in spring 2003 and $300\,\mathrm{m}$ in spring 2004 (VÅGE ET AL., 2006) - the winter were the data collection of the CIS mooring failed.

3.3 Heat and freshwater fluxes in the Central Irminger Sea

3.3.1 Heat budget

The ocean and atmosphere systems are linked amongst others via fluxes of heat across the ocean-atmosphere interface (MOISAN AND NIILER, 1998). The heat content of a layer can be derived from the vertical integration of the temperature from the bottom of the layer, h, to the sea surface.
According to MOISAN AND NIILER (1998), the rate of change of heat content Q_{net} is given by:

$$Q_{net} \;=\; \rho c_w h \frac{\partial T_a}{\partial t}, \tag{3.1}$$

where ρ is the mean density of seawater, c_w the heat capacity of seawater, h the layer depth and T_a the depth averaged temperature. For the layer depth h a fixed or space- and time-varying depth, e.g. MLD or depth of an isotherm, can be chosen (WIJESKERA AND BOYD, 2001). For the calculations carried out in this study a constant depth of $1000\,\mathrm{m}$ is taken based on the depth of the deepest attached instrument during the first deployment period.

The changes of the heat content is the sum of net heat fluxes across the ocean surface (Q_{srf}), horizontal heat fluxes (Q_{trans}), entrainment (Q_{ent}) and additional heat fluxes across the surface in depth h:

$$Q_{net} \;=\; Q_{srf} + Q_{trans} + Q_{ent} - Q_{-h}. \tag{3.2}$$

The net surface heat flux Q_{srf} is the result of

- short-wave solar irradiance (Q_{sw})
- net long-wave back radiation (Q_{lw})
- sensible heat fluxes (Q_{sen}) due to vertical temperature gradients and
- latent heat fluxes (Q_{lat}) in consequence of vertical humidity gradients in combination with wind,

which can be expressed by the equation:

$$Q_{srf} \;=\; Q_{sw} + Q_{lw} + Q_{sen} + Q_{lat}. \tag{3.3}$$

For estimating these fluxes in the mooring area atmospheric reanalyses data has been taken into account. The net surface heat flux and its components are illustrated in fig. 2.5. Monthly averaged values of Q_{srf} are shown in fig. 3.7 (a).

The next term Q_{trans} represents fluxes due to horizontal heat transport. The values can be negative (inflow of cold water or outflow of warm water) or positive (inflow of warm water or outflow of cold water) (PICKARD AND EMERY, 1990). On the one hand this can be associated with an advective flux that is a result of a mean horizontal current $\mathbf{u}_a$ and a horizontal gradient of the vertically averaged temperature T_a (MOISAN AND NIILER, 1998):

$$Q_{adv} \;=\; \rho c_w h\, \mathbf{u}_a \;\cdot\; \nabla T_a. \tag{3.4}$$

On the other hand it might be induced by a horizontal eddy heat transport:

$$Q_{eddy} \;=\; \rho c_w h\, \nabla \;\cdot\; \left(\int_{-h}^{0} \mathbf{u}' T'\, dz \right) \tag{3.5}$$

with $\mathbf{u}'$ and T' being the deviations from the vertically averaged horizontal velocity $\mathbf{u}_a$ and temperature T_a, respectively. Because a single mooring can not resolve a horizontal field it is not possible to estimate the impact of both parts. BEGLER (2004) used float data in addition to mooring data to achieve the gradients of the mean temperature field. The results implemented that besides the advection with the mean field, the eddy activity influences the horizontal heat transport in this area.

The fluxes due to entrainment are caused by the horizontal and temporal variability of the layer depth as well as vertical currents at this depth combined with the difference between vertically averaged temperature and temperature at depth h:

$$Q_{ent} \;=\; \rho c_w (T_a - T_{-h})(\partial h/\partial t \;+\; \mathbf{u}_{-h} \;\cdot\; \nabla h \;+\; w_{-h}). \tag{3.6}$$

But as the layer depth, that is chosen for the calculations, is constant and the vertical velocity is typically small, the term can be neglected. Calculations of BEGLER (2004) confirm this.

Additional fluxes Q_{-h} across the interface at the layer depth can occur due to penetrating solar radiation and other turbulent or molecular process. These fluxes are difficult to estimate, but on average their contribution can be neglected as well. Fluxes in consequence of penetration for example are negligible because the depth h is always below the main thermocline.

Due to this the rate of change is balanced by the surface heat fluxes and oceanic heat transport that includes advection via mean current and horizontal eddy heat transport:

$$Q_{net} \;=\; Q_{srf} + Q_{trans}. \tag{3.7}$$

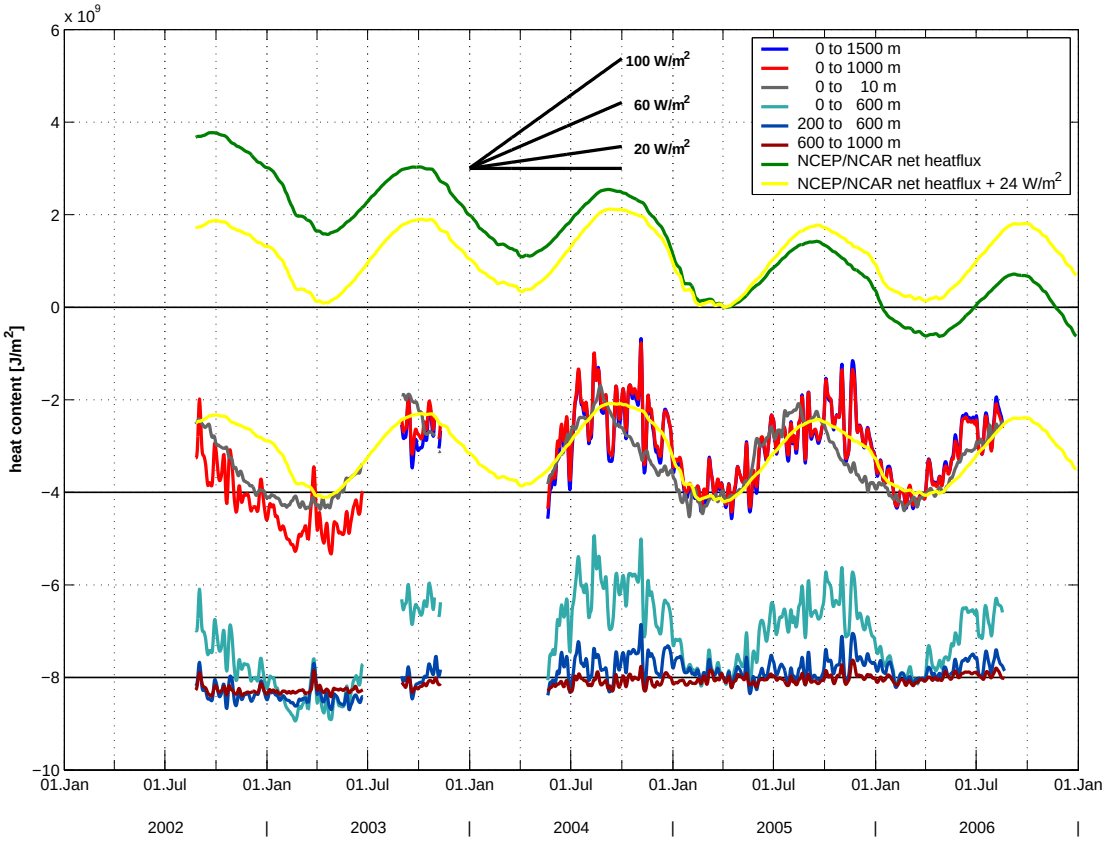

FIGURE 3.6: *Time series of heat content from summer 2002 to summer 2006 at different depths based on mooring measurements. The green line represents the time integral of the net NCEP surface heat fluxes and the yellow line the same fluxes with the overall mean of* $-24\,\mathrm{W/m^2}$ *removed. The heat content was estimated by vertically integrating the observed temperatures over the indicated depths. All time series are offset so that the heat contents match on April 1st 2005.*

Calculations of the heat content over different depth ranges for the mooring period are given in figure 3.6. Additionally the time integral of the net NCEP/NCAR surface heat fluxes are illustrated.
During spring and summer the net heat flux Q_{srf} across the air-sea interface leads to a warming of the water column. In contrast to this there is cooling during autumn and winter. The yearly average reveals a heat loss for this area. For the 4 years (September to August) the NCEP/NCAR reanalyses data based annual average surface heat flux over the central Irminger Sea is $-24\,\mathrm{W/m^2}$. For comparison: estimations for the central Labrador Sea revealed an annual average of $-36\,\mathrm{W/^2}$ between 1996 and 2005 (AVSIC ET AL., 2001).
The seasonal cycle of the heat content shows high variability on short timescales.

The temporary maximum in March 2003 for example is the result of a warm core eddy that extended from near-surface down to $750\,\mathrm{m}$. Nevertheless, the observed heat content of the upper $1000\,\mathrm{m}$ tracks the time integral of the surface flux when the mean surface heat loss for the period summer 2004 to 2006 ($-24\,\mathrm{W/m^2}$) is removed. During the first deployment period it also tracks the line after applying an additional offset. Even the heat content calculated by assuming that the SST is representative for the layer shows a comparable course. Just during the last quarter each year there are differences. The development of the heat content of the layer 600 to $1000\,\mathrm{m}$ shows a steady increase of $\sim 0.4 \times 10^9\,\mathrm{J/m^2}$ within 4 years which is equivalent with an averaged flux of $3\,\mathrm{W/m^2}$. As the deepest MLD did not exceed this depth, the layer is not influenced by surface fluxes. It does not show a seasonal cycle. Thus, the increase reflects the heat storage in the gyre caused by the mixing with the surrounding water.

For a more detailed estimation of the warming and its variability monthly and yearly averages of net surface fluxes and ocean heat transport were determined (figure 3.7). The comparison of the monthly surface heat flux shows that the values between spring and summer of each year are comparable. The difference to the 5-year mean is extremely low at this time (panel b). More variability can be seen during winter. Especially the high heat loss in December 2004 and January 2005 strikes. This is the time when deepest MLD is observed. Although January 2006 shows a similar high value, the established MLD is much shallower and the temperature of the mixed layer is warmer (table 3.1).
The heat flux via ocean heat transport is derived from the difference between the change in heat content over the upper $1000\,\mathrm{m}$ and the surface heat flux. The monthly values varies a lot. But on average $+28\,\mathrm{W/m^2}$ can be associated with a horizontal heat transport. This can be related with an inflow of warm water or an outflow of cold water. The winter months (DJFM) of the first and third year even achieve values of 135 and $59\,\mathrm{W/m^2}$, respectively. The high value of the first year can partly be explained by the occurrence of the already mentioned warm core eddy in March. During the last winter even a small negative heat transport took place, which advocated the establishment of a MLD comparable to the first winter. But this seems to be an exception. Thus, in cases of using a 1-dimensional model a heat flux due to oceanic heat transport should be taken into account.
The residual of averaged atmospheric heat loss and ocean heat transport is $4\,\mathrm{W/m^2}$. This is equivalent with the accumulation of heat in the gyre. The accumulation is a result of the stratification that led to an increase of the mean temperature between 600 to $1000\,\mathrm{m}$. The associated flux in this depth range explains about 75% of the heat storage. Thus, about $1\,\mathrm{W/m^2}$ can be associated with an accumulation of heat in the upper $600\,\mathrm{m}$.

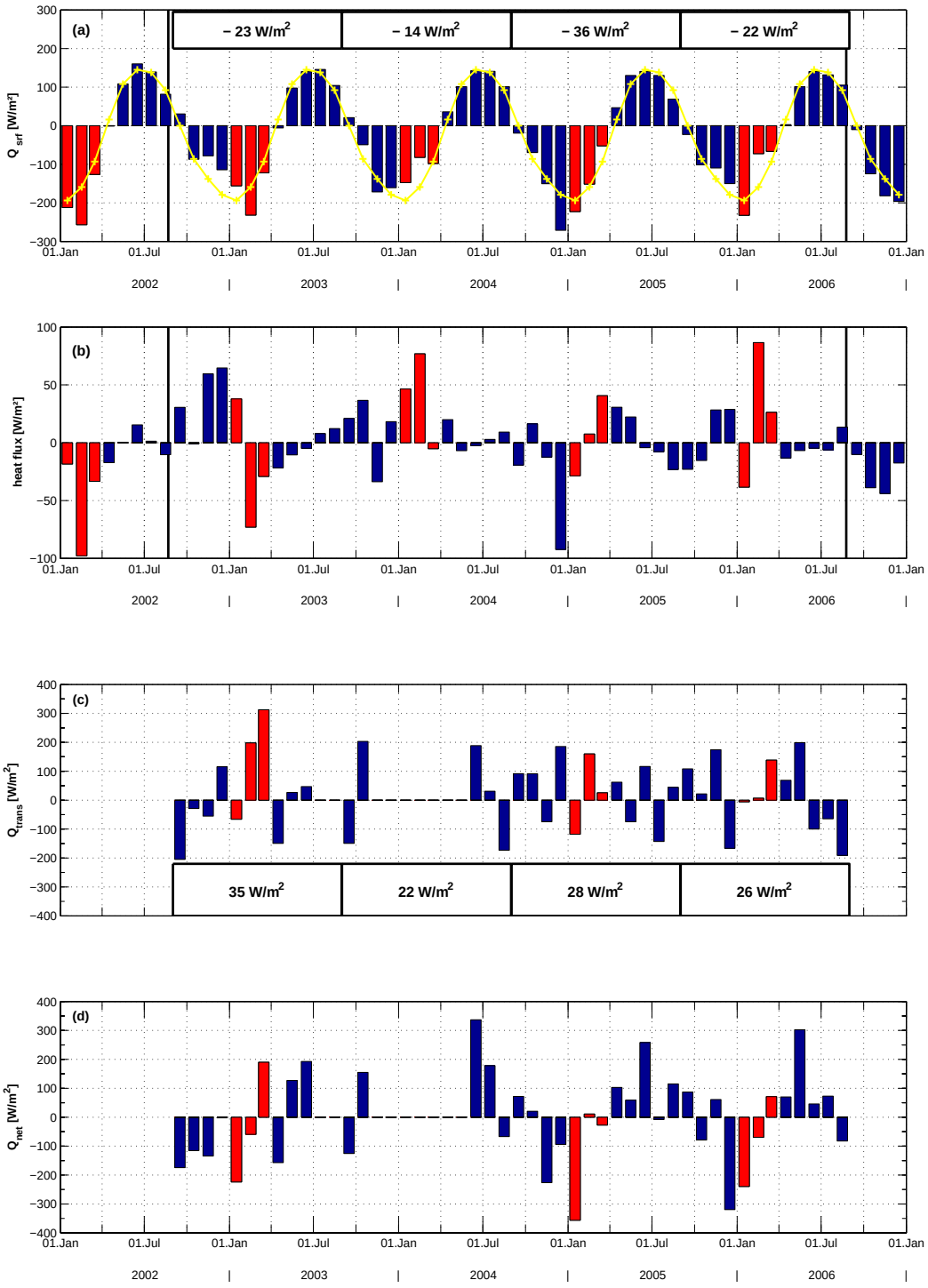

FIGURE 3.7: *Panel (a): Time series of monthly surface heat flux. The yellow line represents the monthly values averaged over the 5 given years. The yearly anomaly for the time September to August is given in the boxes. Panel (b) shows the difference of actual monthly heat flux to 5-year monthly mean. Horizontal heat fluxes and the residual that represents the heat content changes are illustrated in panel (c) and (d), respectively. Values for January to March are marked red.*

3.3.2 Freshwater budget

For an estimation of the freshwater budget the conservation of salt is adopted. Salt is neither gained or lost through the atmosphere. Thus, the increase of salinity in a layer must either be the result of a mixing with additional salt or less freshwater from the surrounding waters, or the remove of freshwater via surface fluxes due to the residual of evaporation E and precipitation P (CURRY ET AL., 2003); river runoff is negligible in this area. Based on the mooring data the rate of salinity change can be calculated by using the equation:

$$\rho_1 S_1 H \;=\; \rho_2 S_2 (H + \Delta h), \tag{3.8}$$

where H is the average thickness of a layer (in cm) and Δh is the height (in cm) of freshwater that was added. The freshwater content can be calculated in the same way when a mean salinity is assumed. In this case Δh represents the anomaly of freshwater relative to the average. The results are illustrated in figure 3.8.

The freshwater content reflects the salinity anomalies of the depth range relative

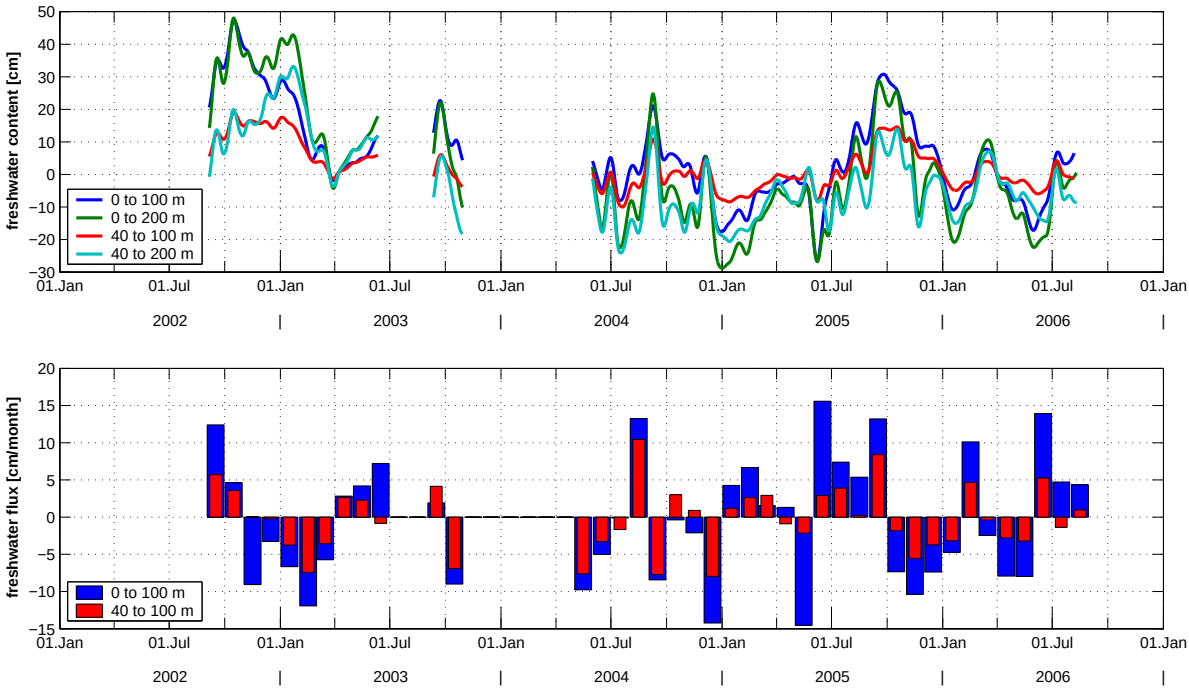

FIGURE 3.8: *Time series of freshwater content for different (near-)surface layers are illustrated in (top panel). The estimation was done by using Eq. 3.8. H represents the layer thickness given by the depth range. For ρ_1 and S_1 constant values of $1027.7\,\mathrm{kg/m^3}$ and 34.9 are assumed, respectively. Data are smoothed over 30 days. The panel below gives the monthly averaged changes in freshwater content based on the results above.*

to an averaged salinity of 34.9. The calculation was done for different surface layer depth ranges. The values of the layer 40 to $100\,(200)\,\mathrm{m}$ is not effected by errors that may occur due to the construction of surface salinity. But especially during the first year this leads to an underestimation of the freshwater anomaly. The origin of this anomaly is not known and can be explained just to a small amount by anomalous high ($E - P$) rate. A possible source might be freshwater that has been advected from the East Greenland Current to the mooring site during summer time.
A comparison of the freshwater content in the upper 100 and $200\,\mathrm{m}$ shows the result of vertical mixing during October 2002 and January 2003. While the content of the upper $100\,\mathrm{m}$ decreases continuously during the period, the volume of freshwater over the upper $200\,\mathrm{m}$ does not change much. During the summer months just slight differences between the layers are detectable. At this time differences mainly occur in consequence of the consideration of the upper $40\,\mathrm{m}$.

Each year between October and January roughly $20\,\mathrm{cm}$ of freshwater has to be removed. But due to the initial state the winterly results differ. Shallowest values occur end of December 2004. This conditions together with the intense heat flux at this time advocated the establishment of a relatively deep mixed layer.
Looking at the changes in the upper $100\,\mathrm{m}$ (lower panel in fig. 3.8) shows that about half of the changes can be explained with variations in shallower depth. Occasionally the content of the upper $40\,\mathrm{m}$ stays stable and the changes are just caused by variations in the layer below.

According to NOAA NCEP EMC CMB GODAS data ($E-P$) in this area is on average about $-0.8\,\mathrm{m/yr}$ for the first two years and $\sim\ 0.5\,\mathrm{m/yr}$ for the period September 2004 to August 2006, which points to a freshwater import due to precipitation. But this does not explain all of the present freshwater in summer 2002 and it must partly be associated with an horizontal transport of freshwater from surrounding waters. In contrary, for the remaining period the presence of relatively saline water must be the result of advected saline water from the surrounding, for example from the Irminger Sea Current.

3.3.3 Combining heat and freshwater fluxes: the buoyancy flux

As already mentioned the deepest MLD within the observed period did not exceed a depth of $600\,\mathrm{m}$. But what is necessary to achieve a deepening of the convecting layer down to over $1000\,\mathrm{m}$ for example, depths that are comparable with those observed in the Labrador Sea? In this case a look at the buoyancy is revealing.

The buoyancy force itself that acts on a water parcel in a column is given by its anomaly in buoyancy relative to the surrounding fluid or a reference water parcel:

$$b \;=\; -g\Big(\frac{\rho'}{\rho_0}\Big) \tag{3.9}$$

where g ($9.81\,\mathrm{m/s^2}$) is the acceleration due to gravity, ρ_0 is a constant reference density ($1027.7\,\mathrm{kg/m^3}$ in the following calculations) and

$$\rho' \;=\; \rho_1 \;-\; \rho_2 \tag{3.10}$$

the density difference between the relevant water parcels. Difficulties arise because the density of seawater depends in complex ways on potential temperature θ, salinity S and pressure p (see VERONIS, 1972):

$$\rho \;=\; \rho(\theta, S, p). \tag{3.11}$$

Therefore, a simplified version (see Eq. (2.1)) is often used in theoretical studies. Using this linearised equation and assuming that α_θ and β_S are almost identical for the two given water parcels that are compared, Eq. (3.9) can be written as:

$$b \;=\; -g[\alpha_\theta(\theta_2 - \theta_1) - \beta_S(S_2 - S_1)] \;\; [^m/_{s^2}] \tag{3.12}$$

and reveals that the buoyancy force consists of a thermal and a haline term.

Equivalent to this the buoyancy flux at the sea surface is expressed in terms of heat and freshwater fluxes:

$$\mathcal{B} \;=\; g\left(\frac{\alpha_\theta}{\rho_0 c_w} Q_{srf} + \beta_S S(E-P)\right) \;\; [^{m^2}/_{s^3}] \tag{3.13}$$

where c_w is the heat capacity of water ($4000\,\mathrm{J\,kg^{-1}\,K^{-1}}$), Q_{srf} the surface heat loss, and $(E-P)$ the difference between evaporation and precipitation that represents the net freshwater flux (MARSHALL AND SCHOTT, 1999).

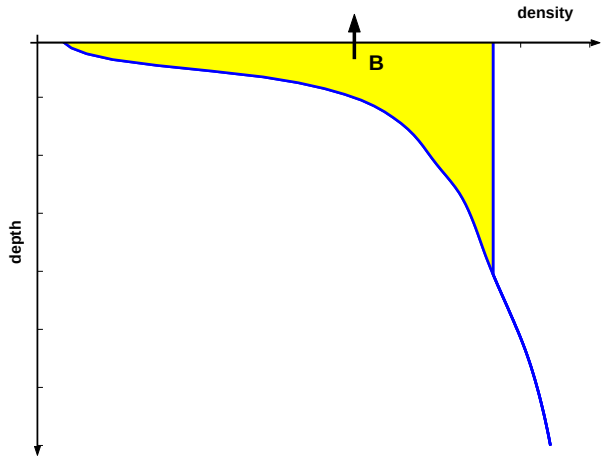

FIGURE 3.9: *Schema for calculating the buoyancy flux*

The vertical integration of buoyancy b from the surface to a given depth H is equal to the integration of buoyancy flux $\mathcal{B}$ over a period t_1 to t_2:

$$B = \int_{t_1}^{t_2} \mathcal{B}\, dt = -\frac{g}{\rho_0} \int_{-H}^{0} [\rho_2(z) - \rho_1(z)]\, dz. \tag{3.14}$$

And, as illustrated schematically in figure 3.9, it is proportional to the area between the two given density profiles. The resulting buoyancy loss B gives the energy that has to be removed from the water column to destabilize the density profile down to the depth H within the given time. This can be realized by cooling or an increase in salinity. As above, the integrated buoyancy can also be divided in a thermal and haline driven term: B_θ and B_S, respectively.

The vertically integrated buoyancy and its components are contoured for the upper $1000\,\mathrm{m}$ in figure 3.10. The estimated MLD is almost identical with a constant value of $0.02\,\mathrm{m}^2/\mathrm{s}^2$. Assuming that the buoyancy loss is solely caused by heat changes from the surface, the loss can be converted to a heat loss of $2.5\,\mathrm{W}/^2$ over one year.

The thermal influence is much higher than the haline as it may have been expected for this area. A relatively strong negative effect of the haline term arises in depth below $\sim\ 650\,\mathrm{m}$ due to the salinity minimum of the LSW. But it occurs mainly during summertime wich is not relevant. Nevertheless increased thermal driven buoyancy flux is necessary in this area to compensate the effect and achieve greater depths.
Regarding this illustrations an integrated buoyancy of $0.4\,\mathrm{m}^2/\mathrm{s}^2$ would be needed to establish a convecting depth greater than $1000\,\mathrm{m}$ during the observed period.

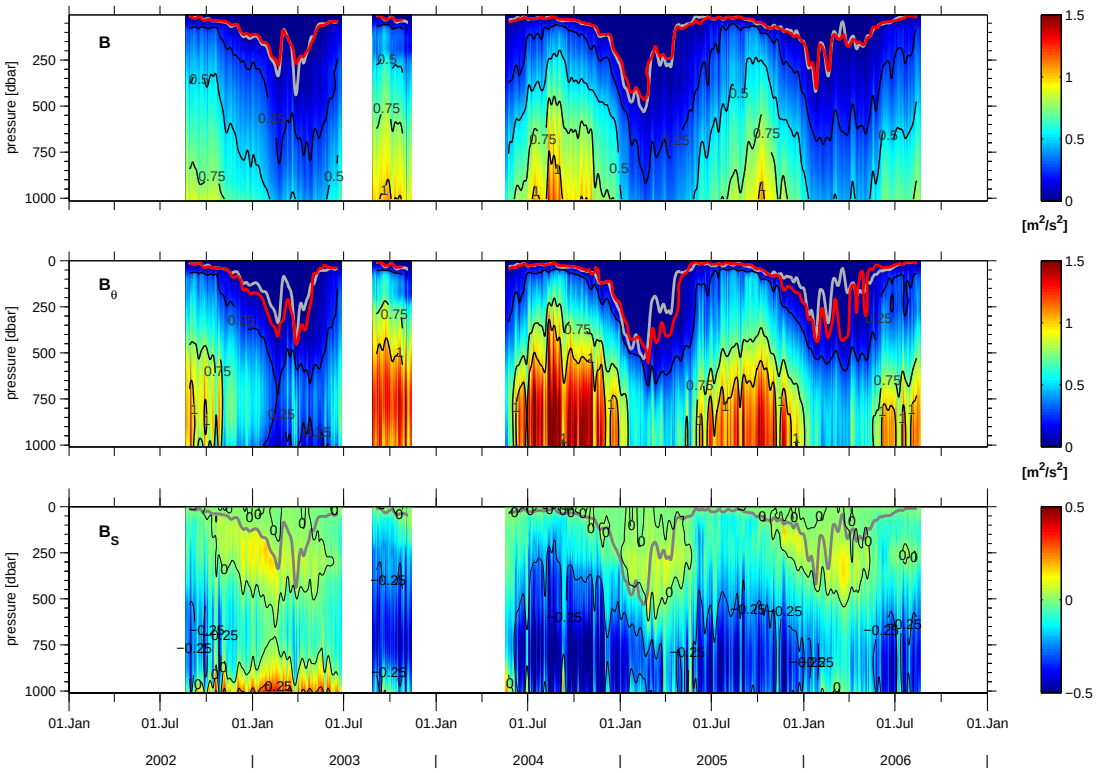

FIGURE 3.10: *Contoured time series of vertically integrated buoyancy B (top panel) as well as its components B_θ and B_S for depth down to $1000\,\mathrm{m}$. The gray line denotes the MLD averaged over 14 days. Smoothed contour levels are given as labeled. The red line represents the contour of $0.02\,\mathrm{m}^2/\mathrm{s}^2$ that is almost identical to the MLD.*

A more obvious estimation for the three winter gives figure 3.11. It shows the vertical distribution of σ_θ as measured during end of summer (blue line) and during winter time when the maximum MLD is established (red line). The black line indicates a hypothetical distribution of an assumed convecting layer that exceeds $1000\,\mathrm{m}$. The area between the red and blue line gives the buoyancy that was removed over the period between September and February. Winter 2002/2003 and 2005/2006 show comparable values. Even the thermal driven buoyancy flux over both periods are almost identical, although during the first winter much more tip jet events could be observed.

By ignoring the effects of evaporation, precipitation and any horizontal heat transport, this can roughly be associated with an additionally needed heat loss of 113, 62 and $124\,\mathrm{W}/\mathrm{m}^2$ from the surface over 6 months for the three observed winters. According to surface heat fluxes taken from NCEP/NCAR reanalyses the heat loss during September and March amounted to 104, 149 and $115\,\mathrm{W}/\mathrm{m}^2$ for the given

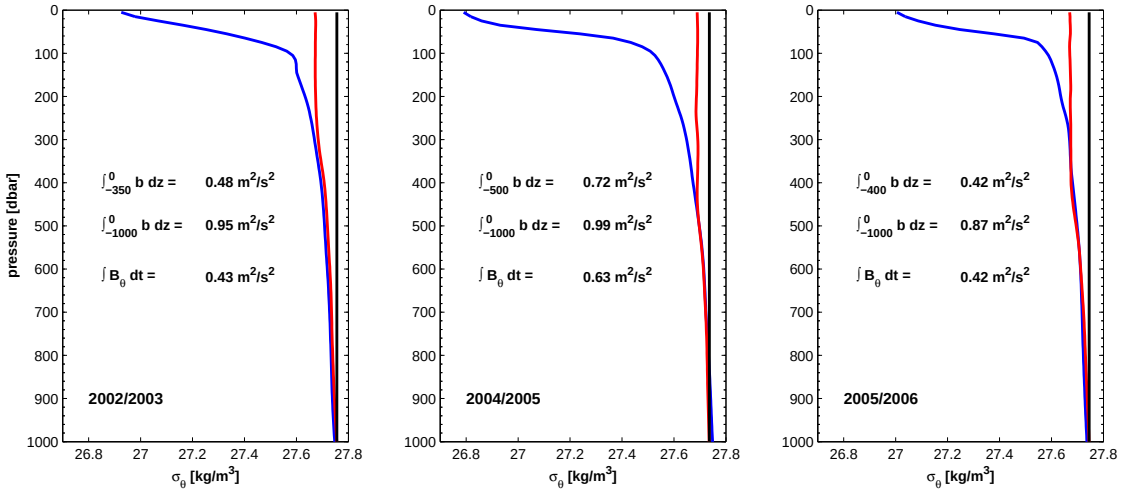

FIGURE 3.11: *Vertical distribution σ_θ as measured during end of summer (blue) and during time with maximum established MLD (red). The black line indicates a hypothetical distribution that assumes a convecting layer exceeding* 1000 m. *Vertically integrated buoyancy down to observed and hypothetical MLD are given as well as the temporally integrated thermal buoyancy flux that is associated with the surface heat flux occurring in the meantime.*

seasons. To achieve a MLD comparable to those observed in the Labrador Sea about half of the actually obtained surface heat flux must have been added in winter 2004/2005. During the other two winters even twice as much would have been needed.

3.4 The influence of prevailing currents

An impression how the prevailing currents may influence the establishment of a mixed layer can be achieved by comparing the development of the MLD in figure 3.4 and the winterly currents illustrated in figure 3.12.
The top panel of fig. 3.12 contains the measured, vertically averaged currents illustrated by a stickplot diagram (data smoothed over 7 days). Furthermore, the absolute velocity (blue), the velocity of the monthly averaged current (red) and the standard deviation of its monthly fluctuations (difference between red and yellow line) are plotted. The four panels below show the horizontal displacement due to constant monthly mean currents, while the four panels at the bottom represents the same caused by monthly fluctuations during the 4 winters. Each season (September to March) is labeled in all panels. The coloured dots that occur every 7th day indicate the day of the season.
In general the horizontal displacement due to the mean current is low during December and/or January. The displacement in consequence of current fluctuations varies strongly. Weakest monthly mean current together with little fluctuations can for example be found in December 2004 and January 2005 (period (c)). A look at the progressive vector diagrams show that the horizontal displacement was less than $50\,\mathrm{km}$ over these two months. The advective term of the heat balance (fig. 3.7) points to a slight negative value. At this time the mixed layer reached the maximum depth. As the weak current persisted for a few weeks, the mixed layer was not disturbed immediately after the establishment. Just a short time after that the current increased strongly and near-surface freshwater cells entered the mooring site which involves a shallower MLD. Comparable events are visible in early March 2003 and 2006. Even the opposite situation can be detected end of March 2003. A warm core eddy carrying anomalous warm and saline water passes the mooring site. Due to the homogenized pattern the MLD shows a second maximum.

If the gradient of the monthly averaged temperature and salinity field would be known, the heat and freshwater fluxes due to the mean current and due to eddy activity could be estimated. Data that might provide the additional needed information are not included at this state of the study .

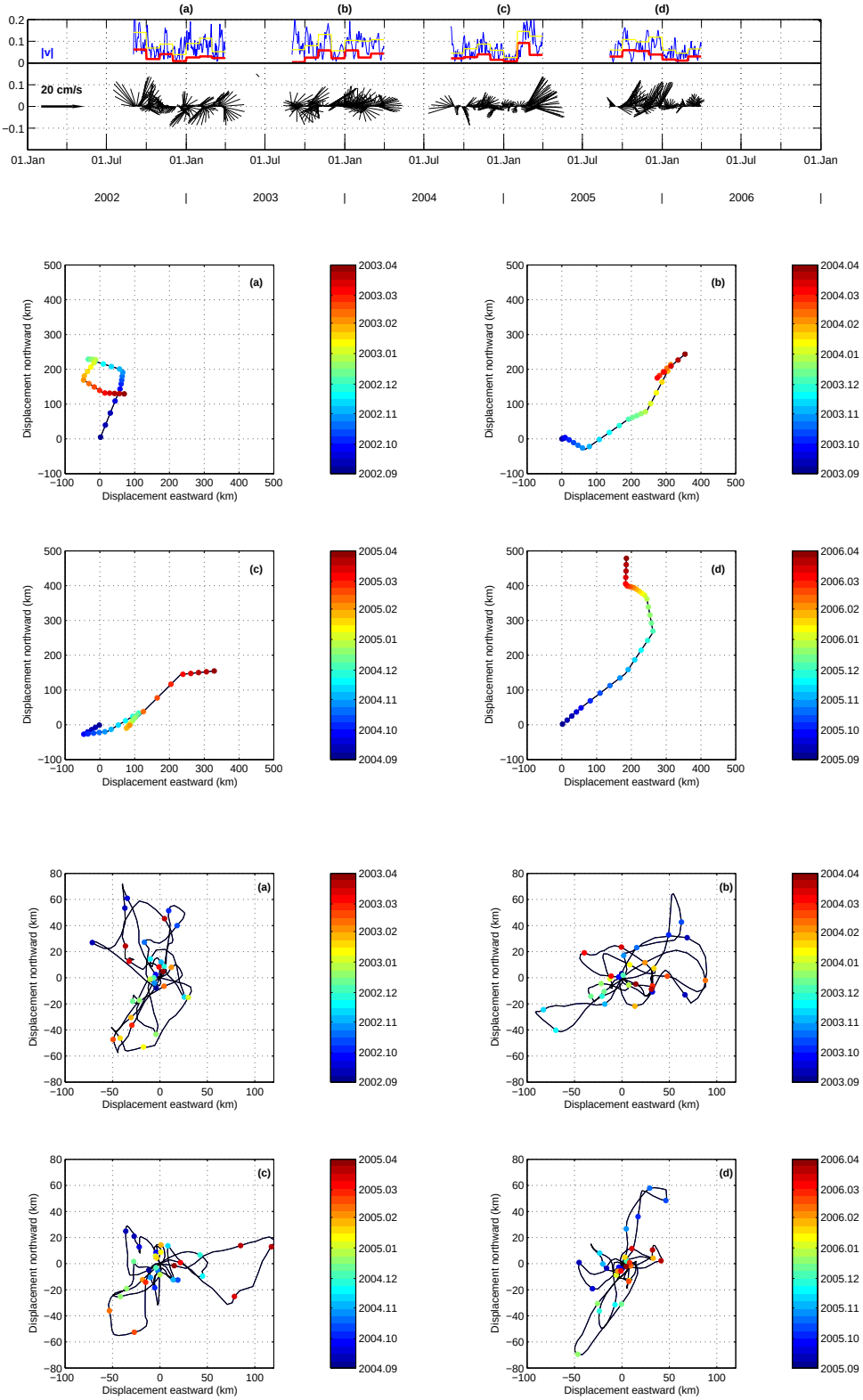

FIGURE 3.12: *Illustration of currents as observed during wintertime and horizontal displacement caused by monthly mean current and monthly fluctuations. For details see text.*

4 Conclusions and Outlook

Data collected in the Central Irminger Sea between summer 2002 and summer 2006 were evaluated regarding the evolution of the physical properties. The circumstances that may influence the convecting activity in this area were in the focus of interest. The three observed winters showed varying situations. The results are listed in table 4.1.

Year	2002/2003	2003/2004	2004/2005	2005/2006
MLD Jan/Feb [m]	350	*300*$^{(a)}$	500	400
σ_0 of mixed layer [kg/m^3]	27.68_1		27.68_4	27.67_0
velocity of mean current [cm/s]				
DJFM	1.4	2.4	2.4	2.2
Jan	2.6	5.8	0.8	1.6
Feb	3.0	2.5	9.2	1.1
salinity$_{0-50m}$ Dec average	34.79_1	(34.87_2)	34.92_0	34.87_8
$\hookrightarrow$ preconditioning	-	+	+	+
NAO DJFM (station based)	0.20	-0.07	0.12	-1.09
NAO DJFM (according to Osborn)	*0.40*	*-0.20*	*-0.11*	*-0.82*
Tip Jets DJFM (days)	13	2	11	3
Q_{srf} DJFM [W/m^2]	-158	-124	-176	-131
Q_{trans} DJFM [W/m^2]	135	n.a.	59	-7
$Q_{\partial W/\partial t}$ DJFM [W/m^2]	-23	n.a.	-117	-138
Q_{srf} [W/m^2] Sep-Aug	-23	-14	-36	-22
Q_{trans} [W/m^2] Sep-Aug	35	22	28	26
$Q_{\partial W/\partial t}$ [W/m^2] Sep-Aug	12	8	-8	4

TABLE 4.1: *Summary of conditions in the Irminger Sea as observed during summer 2002 and summer 2006; DJFM gives mean of December, January, February and March.*
$^{(a)}$ *adopted from* VÅGE ET AL. *(2006)*

Deepest mixed layer was observed in winter 2004/2005. This winter started with a well preconditioned water column, several tip jet events occurred that enhanced the surface heat flux and stirring, and especially in January the velocity of the mean current and its fluctuations were considerable weak. This favoured a deeper established MLD than in the other observed winters.

As it may have been assumed, the salinity effect on density is not remarkable in this area. But as can be seen from the first winter a freshwater anomaly near the surface can hinder the deepening of the mixed layer and should not be underestimated.
Besides the preconditioning the mean current also seems to influence not only the deepening of the mixed layer. It also has an effect on the stability of the established depth. Weak mean currents with low fluctuations apparently advantages the establishment of an almost constant depth for more than just a few days during times of high surface heat fluxes.
For establishing a convecting depth greater than $1000\,\mathrm{m}$ during the time of observation an additional buoyancy loss of 0.25 to $0.45\,\mathrm{m^2/s^2}$ over the period September to February would have been necessary. By ignoring the effects of evaporation, precipitation and any horizontal transport, this can roughly be associated with an additionally needed heat loss of 70 to $120\,\mathrm{W/m^2}$ from the surface over these 6 months. This is half to twice as much heat loss as it was actually obtained during this time. Because according to surface heat fluxes taken from NCEP/NCAR reanalyses the heat loss during September and March amount on average to $\sim 140\,\mathrm{W/m^2}$ for the years 2002 to 2006.
According to the present observation it seems suspicious that deep convection will take place in the central Irminger Sea in the near future (ignoring the haline contribution to the buoyancy flux). Even if a deep reaching mixed layer may be established the resulting seawater properties will probably not be comparable with those that are associated with uLSW.
Nevertheless, it could be interesting to include the data of the current deployment. Winter 2006/2007 is associated with a high NAO index. According to OSBORN (2007) the index achieved a DJFM mean of $+1.83$; for comparison the value was -0.82 in winter 2005/2006. This may have led to an enhanced appearance of tip jet events and thus to higher turbulent heat fluxes. A well-established MLD could be expected. A comparison with the already observed winters might further lighten which process has the most important influence on convecting activity in the Irminger Sea.

For further investigation of the heat fluxes float data should be taken into account according to the method described by BEGLER (2004) to estimate the horizontal gradient of the monthly averaged temperature and salinity. An estimation of the monthly fluctuations of these property fields seems to be challenging because the temporal resolution of the float data are not satisfactory. Besides this, it might be worthy to reveal an estimation of the term that is driven by the mean current, just as already done by BEGLER (2004) for the first mooring period. Together with the knowledge about the monthly current fluctuations the impact of eddy activity on the ocean heat transport in this area could be investigated.

5 Acknowledgements

Financial support from the European Commission for the CIS mooring site under the FP5-ANIMATE project (EVR1-CT-2001-40014) and FP6-MERSEA I/P project (SiP3-CT-2003-502885) is acknowledged.
The NCEP/NCAR reanalysis data are provided by the NOAA/OAR/ESRL PSD, Boulder, Colorado, USA, from their Web site at *http://www.cdc.noaa.gov*.
NOAA_OI_SST_V2 data provided by the NOAA/OAR/ESRL PSD, Boulder, Colorado, USA, are available at *http://www.cdc.noaa.gov/*.
The NOAA NCEP EMC CMB GODAS monthly surface data are served from IRI/LDEO Climate Data Library (*http://iridl.ldeo.columbia.edu/*).
The QuikScat data are produced by Remote Sensing Systems and sponsored by the NASA Ocean Vector Winds Science Team. Data are available at *http://www.remss.com*.
Microwave OI SST data are produced by Remote Sensing Systems and sponsored by National Oceanographic Partnership Program (NOPP), the NASA Earth Science Physical Oceanography Program, and the NASA REASoN DISCOVER Project. Data are also available at *http://www.remss.com*. Research into SST blending, diurnal warming, observation errors, and near real-time validation of TMI and AMSR-E SST is supported by the NASA ESE Physical Oceanography Program (Dr. Eric Lindstrom) and the NASA ESE AMSR-E Science Team (Dr. Ramesh Kakar). The distribution, web-interface, and visualization tools for these data sets are supported by the NASA ESE REASoN Project (Dr. Lucia Tsaoussi). The scientists working on the production and dissemination of these data are Chelle L. Gentemann, Lucrezia Ricciardulli, Marty Brewer, and Frank J. Wentz of Remote Sensing Systems.

Thanks

to all the people that supported me while working on this Diploma thesis;

to Martin Visbeck, Johannes Karstensen and Uwe Send for supervision and helpful comments;

to Gerd Krahmann, Kerstin Schepanski and Sunke Schmidt for their help with more or less big technical problems and their patient answers on my questions;

to Julia Dettmann and Claudia Denker for reading several chapters and taking care of correct spelling;

and finally to my family and friends for their support during all the time of my study.

Abbreviations

ADCP	Acoustic Doppler Current Profiler
AMSR-E	advanced Microwave Scanning Radiometer
ANIMATE	Atlantic Network of Interdisciplinary moorings and times-series for Europe
CIS	Central Irminger Sea; name of the mooring site
CGFZ	Charlie Gibbs Fracture Zone
CMB	Climate Modeling Branch
DJFM	mean of December, January, February and March
DSOW	Denmark Strait Overflow Water
DWBC	Deep Western Boundary Current
EGC	East Greenland Current
EMC	Environmental Modeling Center
GODAS	Global Ocean Data Assimilation System
ISW	Irminger Sea Water
lLSW	lower Labrador Sea Water
LR	ADCP Longranger
LSW	Labrador Sea Water
LOCO	Long-Term Ocean Climate Observations
MERSEA	Marine environment and security for the European Area
MC	Micro Conductivity and Temperature Recorder (MicroCAT)
MLD	Mixed Layer Depth
MW	Microwave
NAC	North Atlantic Current
NADW	North Atlantic Deep Water
NAO	North Atlantic Oscillation
NCAR	National Center for Atmospheric Research
NCEP	National Center for Environmental Prediction
NEADW	North East Atlantic Deep Water
NOAA	National Oceanic and Atmospheric Adminstration
OI	Optimally Interpolated
RSS	Remote Sensing Systems
SSS / SST	sea surface salinity / temperature
uLSW	upper Labrador Sea Water
WHOI	Woods Hole Oceanographic Institution

Bibliography

AVSIC, T., J. KARSTENSEN, U. SEND and J. FISCHER, 2001: Interannual variability of newly formed Labrador Sea Water from 1994 to 2005. *Geophysical Research Letters*, **33**, L21S02.

BACON, S., W. J. GOULD and Y. JIA, 2003: Open-ocean convection in the Irminger Sea. *Geophysical Research Letters*, **30** (5), p. 1246 et seqq.

BEGLER, C., 2004: Synergie von Zeitserien, Float- und Gleiterbeobachtung mit Anwendung auf den Nordatlantik. Diploma thesis, University of Kiel, 52pp.

BÖHME, L., 2003: Quality Control of Profiling Float Data in the Subpolar North Atlantic. Diploma thesis, University of Kiel, 80pp.

BRONSTEIN, 1997: *Taschenbuch der Mathematik*. Verlag Harri Deutsch, Thun, Frankfurt am Main, 3rd Edition.

CLARKE, R. A. and J.-C. GASCARD, 1983: The formation of Labrador Sea water,Part I, large-scale processes. *Journal of Physical Oceanography*, **13**, p. 1764–1788.

CURRY, R., B. DICKSON and I. YASHAYAEV, 2003: A change in the freshwater balance of the Atlantic Ocean over the past four decades. *Nature*, **426**, p. 826–829.

CURRY, R. and C. MAURITZEN, 2005: Dilution of the Northern North Atlantic in Recent Decades. *Science*, **308**, p. 1772–1774.

DE JONG, M. F. and H. M. VAN AKEN, 2006: Variability and possible convective mixing in the Irminger Sea. internet publication, `www.ifm-geomar.de/index.php?id=poster-list`.

DOYLE, J. and M. SHAPIRO, 1999: Flow response to large-scale topography: the Greenland tip jet. *Tellus*, **51**, p. 728–748.

FALINA, A., 2007: Variability and renewal of Labrador Sea Water in the Irminger Basin in 1991-2004. *Journal of Geophysical Research*, **112**, C01006.

KALNAYA E,. ET AL., 1996: The NCEP/NCAR 40-year reanalysis project. *Bulletin of the American Meteorological Society*, **77**, p. 437–470.

KANZOW, T., 2004: Monitoring the Integrated Deep Meridional Flow in the Tropical North Atlantic. Dissertation, University of Kiel, 140pp.

KARA, A. B., P. A. ROCHFORD and H. E. HURLBURT, 2000: An optimal definition for ocean mixed layer depth. *Journal of Geophysical Research*, **105** (C7), p. 16803–16821.

KARSTENSEN, J., 2005: ANIMATE Report: Calibration of Physical Data. Report, Leibniz Institute of Marine Sciences.

KARSTENSEN, J., T. AVSIC, J. FISCHER and U. SEND, 2006: Subsurface temperature maxima in the Labrador Sea and the Subpolar North Atlantic. *Geophysical Research Letters*, **33**, L21S05.

KISTLER, R., E. KALNAY, W. COLLINS, S. SAHA, G. WHITE, J. WOOLEN, M. CHELLIAH, W. EBISUZAKI, M. KANAMITSU, V. KOUSKY, H. VAN DEN DOOL, R. JENNE and M. FIORINO, 2001: The NCEP-NCAR 50-Year Reanalysis: Monthly Means CD-Rom and Documentation. *Bulletin of the American Meteorological Society*, **82** (2), p. 247–267.

KOLTERMANN, K. P., A. V. SOKOV, V. P. TERESCHENKOV, S. A. DOBROLIUBOV, K. LORBACHER and A. SY, 1999: Decadal changes in the thermohaline circulation of the North Atlantic. *Deep-Sea Research II*, **46**, p. 109–138.

LAVENDER, K. L., R. E. DAVIS and W. B. OWENS, 2000: Mid-depth recirculation observed in the interior Labrador and Irminger sea by direct velocity measurements. *Nature*, **407**, p. 66–69.

LAZIER, J. R. N., 2001: "Deep Convection". In: *Encyclopedia of Ocean Sciences*, J. H. Steele, S. A. Thorpe and K. K. Turekian, Ed., Academic Press, volume 2, p. 634–643.

LILLY, J. M., P. B. RHINES, M. VISBECK, R. DAVIS, J. R. N. LAZIER, F. SCHOTT and D. FARMER, 1999: Observing Deep Convection in the Labrador Sea during Winter 1994/1995. *Journal of Physical Oceanography*, **29** (8), p. 2065–2098.

LORBACHER, K., D. DOMMENGET, P. NIILER and A. KÖHL, 2006: Ocean mixed layer depth: A subsurface proxy of ocean-atmosphere variability. *Journal of Geophysical Research*, **0** (0), p. 0, accepted January 17, 2006.

MARSHALL, J. and F. SCHOTT, 1999: Open-Ocean convection: Observations, theory, and models. *Reviews of Geophysics*, **37** (1), p. 1–64.

MEDOC GROUP, 1970: Observation of formation of deep water in the Mediterranean Sea. *Nature*, **227**, p. 1037–1040.

MERTENS, C., 2000: Open-Ocean convection in the Labrador and Greenland Seas: Plume Scales and Interannual Variabillity. Dissertation, University of Kiel, 134pp.

MOISAN, J. R. and P. P. NIILER, 1998: The Seasonal Heat Budget of the North Pacific: Net Heat Flux and Heat Storage Rates (1950-1990). *Journal of Physical Oceanography*, **28**, p. 401–421.

MOORE, G. W. K., 2003: Gale force winds over the Irminger Sea to the east of Cape Farewell, Greenland. *Geophysical Research Letters*, **30** (17), p. 1894 et seqq.

MOORE, G. W. K. and I. A. RENFREW, 2005: Tip Jets and Barrier Winds: A QuikSCAT Climatology of High Wind Speed Events around Greenland. *Journal of Climate*, **18** (18), p. 3713–3725.

NANSEN, F., 1912: Das Bodenwasser und die Abkühlung des Meeres. *Internationale Revue der gesamten Hydrobiologie und Hydrographie*, **5** (1), p. 1–42.

NOAA CLIMATE DIAGNOSTIC CENTER, 2004: The NCEP/NCAR Reanalysis Project. internet publication,
www.cdc.noaa.gov/cdc/data.ncep.reanalysis.html.

NOAA NATIONAL CLIMATE LABORATORY, 2004: World Ocean Atlas 2001. internet publication,
www.nodc.noaa.gov/OC5/WOA01/pr_woa01.html.

OSBORN, T., 2007: Tim Osborn: North Alantic Oscillation index data. internet publication,
www.cru.uea.ac.uk/~timo/projpages/nao_update.htm.

PICKARD, G. L. and W. J. EMERY, 1990: *Descriptive physcial oceanography: an introduction*. Butterworth-Heinemann, 5th Edition.

PICKART, R. S., M. A. SPALL, M. H. RIBERGAARD, G. W. K. MOORE and R. F. MILLIFF, 2003a: Deep Convection in the Irminger Sea forced by the Greenland tip jet. *Nature*, **424**, p. 152–156.

PICKART, R. S., F. STRANEO and G. W. K. MOORE, 2003b: Is Labrador Sea Water formed in the Irminger Basin? . *Deep-Sea Research I*, **50** (1), p. 23–52.

POND and G. L. PICKARD, 1983: *Introductory Dynamical Oceanography*. Butterworth-Heinemann, 2nd Edition.

REMOTE SENSING SYSTEMS, 2006a: Description of Microwave OI SST Data. internet publication,
www.remss.com/sst/microwave_oi_sst_data_description.html.

REMOTE SENSING SYSTEMS, 2006b: Description of Scatterometer Data Products. internet publication,
www.remss.com/qscat/qscat_description.html.

RENFREW, I., G. MOORE, P. GUEST and K. BUMKE, 1994: A Comparison of Surface Layer and Surface Turbulent Flux Observations over the Labrador Sea with ECMWF Analyses and NCEP Reanalyses. *Journal of Physical Oceanography*, **32** (2), p. 383–400.

REYNOLDS, R. W., 1988: A real-time gloabla sea surface temperature analysis. *Journal of Climate*, **1**, p. 75–86.

REYNOLDS, R. W., N. A. RAYNER, T. M. SMITH, D. C. STOKES and W. WANG, 2000: An Improved In Situ and Satellite SST Analysis for Climate. *Journal of Climate*, **15**, p. 1609–1625.

REYNOLDS, R. W. and T. M. . SMITH, 1994: An Improved global sea surface temperature analysis using optimum interpolation. *Journal of Climate*, **7**, p. 929:948.

RRS DISCOVERY CRUISE REPORT, 2006: Cruise Report No. 11, RRS Discovery Cruise 309-310. Report, National Oceanography Centre, Southampton, chapter 4 "IFM-GEOMAR Activities" by J. Karstensen.

SCHMIDT, S., 2003: Süßwassereinflüsse auf die Konvektionsakitivität in der Labradorsee. Diploma thesis, Kiel, 81pp.

SCHOTT, F. A., R. ZANTOPP, L. STRAMMA, M. DENGLER, J. FISCHER and M. WIBAUX, 2004: Circulation and Deep-Water Export at the Western Exit of the Subpolar North Atlantic. *Journal of Physical Oceanography*, **34** (4), p. 817–843.

SFB 460, 2007: Sonderforschungsbereich 460: Dynamics of Thermohaline Circulation Variability. internet publication.

SMITH, S. R., D. M. LEGLER and K. V. VERZONE, 2001: Quantifying Uncertainties in NCEP Reanalysis Using High-Quality Research Vessel Obesrvations. *Journal of Climate*, **14** (20), p. 4062–4073.

SOLOVIEV, A. and B. KLINGER, 2001: "Open Ocean Convection". In: *Encyclopedia of Ocean Sciences*, J. H. Steele, S. A. Thorpe and K. K. Turekian, Ed., Academic Press, volume 4, p. 2015–2022.

SPALL, M. A. and R. S. PICKART, 2003: Wind-driven recirculation and exchange in the Labrador and Irminger Sea. *Journal of Physical Oceanography*, **33** (8), p. 1829–1845.

SY, A., M. RHEIN, J. R. N. LAZIER, K. P. KOLTERMANN, J. MENCKE, A. PUTZKA and M. BERSCH, 1997: Surprisingly rapid spreading of newly formed intermediate waters across the North Atlantic Ocean. *Nature*, **386**, p. 675–679.

TOMCZAK, M. and J. S. GODFREY, 2005: *Regional Oceanography: An Introduction*. first edition published by Pergamon, now online pdf version, `www.es.flinders.edu.au/ mattom/regoc/pdfversion.html`.

VÅGE, K., R. S. PICKART, G. W. K. MOORE and M. H. RIBERGAARD, 2006: Winter mixed-layer development in the central Irminger Sea: The effect of strong, intermittent wind events. submitted to Journal of Physical Oceanography.

VÅGE, K., R. S. PICKART, G. W. K. MOORE, M. H. RIBERGAARD and H. C. DAVIES, 2007: The Greenland Tip Jet and its Effect on the Irminger Sea. poster presentation, `www.ifm-geomar.de/index.php?id=poster-list`.

VERONIS, G., 1972: On properties of sea water defined by temperture, salinity and pressure. *Journal of Marine Research*, **30**, p. 227–255.

VISBECK, M., 1993: Konvektion im offenen Ozean - Interpretation vonBeobachtungen aus der Grönlandsee und dem westlichen Mittelmeer. Report 237, Berichte aus dem IfM Kiel.

WIJESKERA, H. and T. J. BOYD, 2001: "Upper Ocean Heat and Freshwater Budgets". In: *Encyclopedia of Ocean Sciences*, J. H. Steele, S. A. Thorpe and K. K. Turekian, Ed., Academic Press, volume 6, p. 3079–3083.

Erklärung

Hiermit bestätige ich, dass ich die vorliegende Diplomarbeit selbständig verfasst und keine anderen als die angegebenen Quellen und Hilfsmittel verwendet habe. Ich versichere, dass diese Arbeit noch nicht zur Erlangung eines Diplomgrades an anderer Stelle vorgelegen hat.

Kiel, Mai 2007

(Uta Neumann)